

Intrinsic blood–brain barrier dysfunction contributes to multiple sclerosis pathogenesis

Hideaki Nishihara,^{1,†} Sylvain Perriot,² Benjamin D. Gastfriend,³ Marel Steinfort,¹ Celine Cibien,¹ Sasha Soldati,¹ Kinya Matsuo,¹ Sarah Guimbal,¹ Amandine Mathias,² Sean P. Palecek,³ Eric V. Shusta,^{3,4} Renaud Du Pasquier² and Britta Engelhardt¹

1 Theodor Kocher Institute, University of Bern, Switzerland

2 Laboratory of Neuroimmunology, Lausanne University Hospital (CHUV) and University of Lausanne, Lausanne, Switzerland

3 Department of Chemical and Biological Engineering, University of Wisconsin-Madison, WI, USA

4 Department of Neurological Surgery, University of Wisconsin-Madison, WI, USA

[†]Present Address: Yamaguchi University, Department of Neurotherapeutics, Yamaguchi, Japan

Correspondence to: Prof. Dr Britta Engelhardt

Theodor Kocher Institute

University of Bern

Freiestrasse 1

3012 Bern

Switzerland

E-mail: bengel@tki.unibe.ch

Correspondence may also be addressed to: Dr Hideaki Nishihara

E-mail: hidehara@yamaguchi-u.ac.jp

Running title: Intrinsic BBB alteration in MS

1 Abstract

2 Blood-brain barrier (BBB) breakdown and immune cell infiltration into the central nervous system (CNS)
3 are early hallmarks of multiple sclerosis (MS). The mechanisms leading to BBB dysfunction are
4 incompletely understood and generally thought to be a consequence of neuroinflammation. Here, we
5 have challenged this view and asked if intrinsic alterations in the BBB of MS patients contribute to MS
6 pathogenesis. To this end, we made use of human induced pluripotent stem cells (hiPSCs) derived from
7 healthy controls (HC) and MS patients and differentiated them into brain microvascular endothelial cell
8 (BMEC)-like cells as *in vitro* model of the BBB. MS-derived BMEC-like cells showed impaired junctional
9 integrity, barrier properties and efflux pump activity when compared to HC. Also, MS-derived BMEC-like
10 cells displayed an inflammatory phenotype with increased adhesion molecule expression and immune
11 cell interactions. Activation of Wnt/ β -catenin signaling in MS-derived endothelial progenitor cells
12 enhanced barrier characteristics and reduced the inflammatory phenotype. Our study provides evidence
13 for an intrinsic impairment of BBB function in MS patients that can be modeled *in vitro*. Human iPSC-
14 derived BMEC-like cells are thus suitable to explore the molecular underpinnings of BBB dysfunction in
15 MS and will assist in the identification of potential novel therapeutic targets for BBB stabilization.

16 **Keywords:** multiple sclerosis; blood-brain barrier; human induced pluripotent stem cells; immune cell
17 migration; permeability

18 **Abbreviations:** ACKR1 = atypical chemokine receptor 1; ALS = amyotrophic lateral sclerosis; BBB = blood-
19 brain barrier; BMEC = brain microvascular endothelial cell; CM = conditioned medium; DMM = defined
20 medium method; DMT = disease-modifying treatment; EAE = experimental autoimmune
21 encephalomyelitis; EECM = Extended endothelial cell culture method; EPCs = endothelial progenitor
22 cells; FBS = fetal bovine serum; GSK-3 = Glycogen synthase kinase-3; GWAS = genome-wide association
23 studies; HC = healthy controls; hiPSCs = human induced pluripotent stem cells; ICAM-1 = intercellular
24 adhesion molecule-1; NaFl = sodium fluorescein; MS = multiple sclerosis; NS = non-stimulated; PBMCs =
25 peripheral blood mononuclear cells; Pe = permeability coefficient; P-gp = P-glycoprotein; RR-MS =
26 relapsing-remitting multiple sclerosis; RT = room temperature; SMLC = smooth muscle-like cell; SNPs =
27 single nucleotide polymorphisms; TEER = transendothelial electrical resistance; Th cells = T helper cells;
28 UMM = unconditioned medium method; VCAM-1 = vascular cell adhesion molecule-1

29

1 Introduction

2 Multiple sclerosis (MS) is considered an autoimmune disorder affecting the central nervous system
3 (CNS), which is caused by the interplay of environmental risk factors and a complex genetic background
4 with now more than 230 quantitative trait loci characterized in genome-wide association studies
5 (GWAS) based on single nucleotide polymorphisms (SNPs).^{1,2} MS currently affects 2.3 million people
6 worldwide, but as the etiology remains unknown, there is no curative treatment available.³ Although
7 targeting immune cell trafficking across the blood-brain barrier (BBB), or even depleting immune cell
8 subsets, showed remarkable efficacy for preventing relapses, these therapies are associated with side
9 effects including progressive multifocal leukoencephalopathy and show limited impact on the
10 progressive disease phase. It is widely accepted that immune cell trafficking into the CNS and focal
11 breakdown of the endothelial BBB are initial hallmarks of MS pathogenesis. Focal BBB dysfunction is
12 visualized by gadolinium-enhanced magnetic resonance imaging (MRI) and occurs early in the
13 pathogenesis of new lesions in MS.⁴ Serial MRI studies have indicated that BBB dysfunction may even
14 precede CNS immune cell infiltration and myelin damage in MS.⁵⁻⁷ Histopathological studies on post-
15 mortem MS brain tissues have provided evidence for continued abnormalities in BBB function during the
16 progressive phase of MS⁸⁻¹² underscoring a central role of BBB dysfunction during the entire course of
17 MS.

18 Current knowledge about the molecular mechanisms mediating BBB dysfunction in MS have to a large
19 degree been derived from animal models, experimental autoimmune encephalomyelitis (EAE), or
20 autopsy and rare biopsy cases of MS brain samples. Post-mortem brain tissue from MS patients
21 displayed reduced or interrupted staining of tight junction and adherens junction proteins like occludin,
22 claudin-5, and VE-cadherin.⁸⁻¹² This picture is associated with fibrinogen and IgG staining outside of
23 blood vessels underscoring the leakage of these serum components across an impaired BBB.¹³
24 Immunostaining for the important efflux pump, P-glycoprotein (P-gp) is also reduced in MS lesions and
25 the function of endothelial P-gp is impaired in EAE.¹⁴ During MS, the endothelial cells of the BBB change
26 their immune phenotype by upregulating intercellular adhesion molecule-1 (ICAM-1), vascular cell
27 adhesion molecule-1 (VCAM-1) and atypical chemokine receptor 1 (ACKR1) in MS lesions^{11,12,15-17}
28 allowing for the infiltration of increased numbers of immune cells into the CNS.

29 However, how these observed BBB alterations precisely contribute to MS pathogenesis, if they are
30 causative or a consequence of CNS inflammation, and what are the molecular underpinnings leading to

1 BBB dysfunction in MS remain unknown. Interestingly first studies performed in animal models have
2 suggested that brain endothelial dysfunction can contribute to the initiation of MS lesion
3 pathogenesis.¹⁸

4 Investigating BBB dysfunction in MS is hampered by the fact that BBB samples from MS brains are not
5 readily accessible for research. While CNS biopsies in the early phase of MS are only performed in
6 atypical cases and may thus not reflect typical MS pathogenesis, autopsy material from the progressive
7 stage of MS mainly reflects the advanced stage of the disease.

8 Recent advancements in stem cell technology have now allowed derivation of human brain
9 microvascular endothelial cell (BMEC)-like cells from human induced pluripotent stem cells (hiPSCs).¹⁹⁻²¹
10 In particular, patient-sourced hiPSC-derived BMEC-like cells uniquely enable the study of BBB
11 dysfunction by providing a scalable and renewable source of BMEC-like cells. Human iPSC-derived *in*
12 *vitro* models of the BBB have been established¹⁹⁻²³ and proven successful to model BBB dysfunction *in*
13 *vitro* in inheritable neurological disorders.²⁴⁻²⁸

14 Since hiPSC-derived CNS cells such as neurons, astrocytes, or oligodendrocytes have proven useful to
15 study MS pathogenesis,²⁹⁻³⁷ we here hypothesized that hiPSC-derived *in vitro* BBB models from MS
16 patients may be useful to understand if intrinsic alterations in BBB function contribute to MS
17 pathogenesis. To this end, we established hiPSCs from MS patients and from healthy controls (HC) and
18 differentiated them into BMEC-like cells using two different methodologies, the Defined Medium
19 Method (DMM)²³ and Extended Endothelial cell Culture Method (EECM).²⁰ All MS-patient derived BMEC-
20 like cells showed impaired barrier properties and an increased inflammatory phenotype. Activating
21 Wnt/ β -catenin signaling restored BBB properties in MS patient-derived BMEC-like cells. Overall, hiPSC-
22 derived BMEC-like cells are thus suitable to model underlying BBB dysfunction in MS and will assist in
23 the identification of potential novel therapeutic targets for BBB stabilization that may be beneficial for
24 treating early and progressive MS.

25 **Materials and methods**

26 **Donors and human induced pluripotent stem cells (hiPSCs)**

27 Three healthy controls (HC) (age/sex: HC1 27/F, HC2 50/M, HC3 49/F) and 4 relapsing-remitting MS (RR-
28 MS) (age/sex: MS1 15/M, MS2 17/F, MS3 21/F, MS4 31/F) patients were enrolled in this study. The

1 blood of all four MS patients, used for human induced pluripotent stem cell (hiPSCs) differentiation, was
2 drawn at the time of their first relapse, prior to starting disease-modifying treatment (DMT).
3 Subsequently all four MS patients were confirmed to suffer from RR-MS and three of them were put on
4 DMT with natalizumab (MS1) or fingolimod (MS2) or dimethyl fumarate (MS3). hiPSCs were
5 reprogrammed, expanded and characterized for pluripotency and differentiation capacity exactly as
6 described before.³² To this end the hiPSC quality has been rigorously assessed according to current good
7 laboratory practice in the field set by an international consortia for clinical use of hiPSCs³⁸ The testing
8 workflow includes assessment of morphology, karyotyping, exclusion of mycoplasma contamination,
9 pluripotency, capability of differentiation and absence of transgenes (episomes). Each cell line passed all
10 these quality criteria and thus ensures that none of the hiPSCs used in this study presented pre-existing
11 aberrations that would bias the results of the study. Six hiPSC clones from 3 HC (2 clones from each
12 donor) and 7 hiPSC clones from 4 MS patients (2 clones from MS1, MS3, and MS4, 1 clone from MS2)
13 were used in this study.

14 **Human Th1* cells for allogeneic T-cell interaction with EECM-BMEC-like cells**

15 Human CD4⁺ T cells were isolated, expanded, and sorted as described in previous studies.³⁹⁻⁴¹ Human
16 Th1* cells were sorted according to their specific expression pattern of chemokine receptors
17 (CXCR3⁺CCR4⁻CCR6⁺) from the buffy coat from blood bank. T cells were thawed one day prior to the
18 respective experiment and labeled with 1 μ M CellTracker™ Green (CMFDA Dye, Life technologies) at
19 37°C (5 % CO₂) for 30 min at the day of the experiment. After labelling, T cells were washed and dead
20 cells were removed by Ficoll-Hypaque gradient (780 g, 20 min, 20 °C). T cells were washed twice and
21 resuspended in migration assay medium (DMEM, 5 % FBS, 4 mM L-Glutamine, 25 mM HEPES) in the
22 appropriate concentration.

23 **Peripheral blood mononuclear cells (PBMCs) for autologous immune cell interaction with EECM- 24 BMEC-like cells**

25 Donors HC2 and MS3 underwent a leukapheresis (consent form 107/13) in the scope to obtain
26 peripheral blood mononuclear cells (PBMCs). PBMCs were isolated from HC2 and MS3 by density
27 gradient centrifugation on Ficoll-Hypaque as described previously⁴² and frozen until use. Due to
28 standard clinical procedure, all three included MS patients who were treatment naïve at the time of the
29 initial blood draw (performed to make hiPSC), were put on treatment shortly afterwards and thus under
30 treatment at the time when PBMCs were isolated for this study. MS1 was under natalizumab treatment

1 and excluded as natalizumab specifically blocks lymphocyte binding to the BBB. MS2 was under
2 fingolimod treatment which prohibited isolating sufficient PBMCs from this patients. We therefore
3 isolated PBMCs from MS3 when she was under dimethyl fumarate treatment and showed no clinical
4 activity for more than three years.

5 **Differentiation of hiPSCs into brain microvascular endothelial cell-like cells (BMEC-like cells)**

6 The previously published Defined Medium Method (DMM)²³ and Extended Endothelial cell Culture
7 Method (EECM)^{20,43} were used to differentiate BMEC-like cells from hiPSCs. To ensure differentiation of
8 hiPSCs to BMEC-like cells in a reproducible manner forming a confluent monolayer with good barrier
9 properties the seeding density for each hiPSC clone was optimized at this step as described^{20,43}. For
10 DMM, hiPSC seeding densities at day -3 or day -4 were optimized at a density between 35,000/cm² to
11 84,000/cm² depending on donor and passage (Supplementary Table 1), in order to obtain reproducible
12 differentiation of DMM-BMEC-like cells forming monolayers with excellent barrier properties as
13 determined by high transendothelial electrical resistance (TEER: > 2,000 Ω×cm²) and low permeability to
14 sodium fluorescein (NaFl, 376.3 Da: Pe NaFl <0.6 × 10⁻⁴ cm/min). Accordingly, for EECM, hiPSC seeding
15 densities at day -3 were optimized to a density between 21,000/cm² to 100,000/cm² depending on
16 donor and passage in order to obtain a high number of endothelial progenitor cells (EPCs)
17 (Supplementary Table 1). EECM-BMEC-like cells at passages between 3-6 were used for assays at day 6
18 after seeding onto Transwell filter inserts at a constant seeding density of 1.12 × 10⁵ cells/500 μl. For co-
19 culture with hiPSC-derived smooth muscle like cells (SMLCs), SMLCs and conditioned medium (CM) from
20 SMLCs were obtained as described before.^{20,43} Transendothelial electrical resistance (TEER) was
21 measured using a Volt-Ohm-Meter (Millicell ERS-2, MERSSTX01-electrode). In order to calculate the net
22 resistance in Ω × cm² of the cell monolayers, TEER value of an empty filter was subtracted from each
23 measurement and TEER values in Ω were multiplied by the surface area of the filters (1.12 cm²) as
24 follows: TEER (Ω×cm²) = (cell monolayer resistance - empty Transwell filter resistance) × surface area
25 (cm²).

26 **Activation of the Wnt/β-catenin signaling pathway in EPCs**

27 Glycogen synthase kinase-3 (GSK-3) inhibitor, CHIR99021 was used as a Wnt/β-catenin pathway
28 activator. Directly after purification by magnetic activated cell sorting, EPCs were treated with 4μM
29 CHIR99021 or DMSO as control in hECSR medium until passage 3 (Figure 5A). Passage 3 EECM-BMEC-like

1 cells were seeded onto Transwell filters and used for permeability assays or adhesion molecule
2 phenotyping as described below.

3 **Permeability assay**

4 Permeability of EC monolayers was assessed by measuring the clearance of sodium fluorescein (NaFl,
5 376.3 Da, Sigma-Aldrich) as previously described.^{20,22,43} Briefly, NaFl was added to the upper
6 compartment of the Transwell inserts at a concentration of 10 μ M. Medium samples containing
7 fluorescent tracer that had diffused across the monolayers were collected from the bottom well every
8 15 min for a total of 60 min, and fluorescence intensity was measured in a Tecan Infinite M1000 multi-
9 well reader (Tecan Trading AG). The experiments were done in triplicates for each condition.

10 **P-glycoprotein function assay (Rhodamine 123 accumulation assays)**

11 P-glycoprotein (P-gp) function was assessed by measuring intracellular accumulation of the P-gp
12 substrate Rhodamine 123 in the presence or absence of the P-gp-specific inhibitor cyclosporin A (CsA) as
13 described before.²² In brief, at day 8 DMM-BMEC-like cells were seeded onto Matrigel coated 24 well
14 plates at a density of 130,000/cm². At day 10, cells were washed with pre-warmed HBSS and pre-
15 incubated with 10 μ M CsA (Sigma C1832) diluted in HBSS or not for 1 hour at 37°C (5% CO₂). Then DMM-
16 BMEC-like cells were incubated with Rhodamine 123 (Sigma 83702) in the presence or absence of CsA
17 for 2 hours at 37°C (5% CO₂). After 2 washes with cold PBS, DMM-BMEC-like cells were lysed with RIPA
18 buffer (Sigma R0278). Intracellular accumulation of the fluorescent Rhodamine 123 was measured using
19 a Tecan plate reader (Infinite M1000). Protein concentrations were measured using a BCA protein assay
20 kit (ThermoFisher Scientific) and Rhodamine 123 fluorescence was normalized to protein concentration
21 for each sample. Percent fold change was calculated by comparing the accumulation of Rhodamine 123
22 in the absence of the P-gp inhibitor CsA of the same cells in parallel.

23 **Investigation of cell surface expression of adhesion molecules by flow cytometry**

24 Cell surface expression of adhesion molecules was investigated as previously described.^{20,43,44} BMEC-like
25 cells differentiated by DMM, or EECM were cultured on Transwell filter inserts in respective media.
26 Some wells were stimulated with 10 ng/mL of recombinant human TNF- α (R&D systems, 210TA) and
27 200 IU/mL recombinant human IFN- γ (R&D systems, 285IF) for DMM-BMEC-like cells, and 1 ng/mL of
28 recombinant human TNF- α (R&D systems, 210TA) and 20 IU/mL recombinant human IFN- γ (R&D

1 systems, 285IF) for EECM-BMEC-like cells for 16 h at 37°C (5% CO₂). Detailed information about
2 antibodies is listed in Supplementary Table 2.

3 **Immunofluorescence stainings and cell size calculation**

4 BMEC-like cells differentiated by DMM, or EECM were cultured on Transwell filter inserts as described
5 previously.^{20,23,43} To stain for claudin-5, occludin, VE-cadherin, cells were fixed with methanol, blocked
6 and permeabilized with 5% skimmed milk containing 0.1 % Triton X-100, and then stained with primary
7 antibodies for 1 hour at RT as described.^{22,23,43,45} After three washes, cells were incubated with
8 respective secondary antibodies for 1 hour at RT. For staining of cell surface ICAM-1 and VCAM-1,
9 primary antibodies were added to live cells and incubated at 37 °C (5% CO₂) for 15 minutes. After
10 washing, cells were fixed with 1% (w/v) formaldehyde, blocked with 5% skimmed milk and then
11 incubated with secondary antibodies as described.^{43,45} Nuclei were stained with DAPI at 1 µg/mL. After
12 washing with DPBS, cell monolayers on filters were mounted with Mowiol (Sigma-Aldrich). Images were
13 acquired using a Nikon Eclipse E600 microscope using the Nikon NIS-Elements BR3.10 software (Nikon,
14 Egg, Switzerland). Detailed information about antibodies is listed in Supplementary Table 2.

15 Average cell numbers and cell sizes per field of view (FOV) were determined using these images of the
16 EECM-BMEC-like cell monolayers stained with DAPI for nuclei and for VE-cadherin, claudin-5 or occludin
17 for endothelial junctions using Fiji image processing. Image noise was reduced by applying the Gaussian
18 Blur filter and separation of overlapping signals was achieved by applying watershed segmentation. The
19 nuclei per FOV were counted using the analyze particles tool of Fiji. The area of each FOV was calculated
20 based on the scale bar included in each image and the mean size of the cells was calculated by dividing
21 the area of each FOV (µm²) with number of nuclei.

22 **Adhesion assays**

23 Adhesion assays were performed as previously described.^{20,43} EECM-BMEC-like cells were cultured on
24 collagen-IV/fibronectin-coated 16-well chamberslides (ThermoFisher) at a density of 75,000/cm² using
25 hECSR medium. Once EECM-BMEC-like cells attached to the chamberslides, hECSR was replaced for
26 SMLC derived conditioned medium (CM) from the same clones. EECM-BMEC-like cells were stimulated
27 or not with 0.1 ng/mL TNF-α + 2 IU/mL IFN-γ for 16 h at 37°C (5% CO₂). 20,000 Th1* cells from allogeneic
28 HC donors were co-incubated with the EECM-BMEC-like cells monolayers at RT for 30 minutes under
29 slight movement using a rocking platform. Chamber slides were gently washed twice and fixed with

1 2.5% glutaraldehyde for 2 hours on ice. Filters were then washed with DPBS, and adherent fluorescence
2 labeled Th1* cells per pre-defined field of view (FOV) were analyzed by fluorescence microscopy (Nikon
3 Eclipse E600) and FIJI software (Version 2.0.0, Image J, USA). Assays were performed in at least
4 quadruplicates in each condition for each experiment.

5 ***In vitro* live cell imaging**

6 *In vitro* live cell imaging of Th1* cell and PBMC interactions with EECM-BMEC-like cells under
7 physiological flow was performed as previously described.²⁰ Briefly, EECM-BMEC-like cells were cultured
8 in cloning rings placed on collagen IV/fibronectin-coated Ibidi μ -dishes (Ibidi). EECM-BMEC-like cells
9 were stimulated with 0.1 ng/ml recombinant human TNF- α + 2 IU/mL IFN- γ for 16 h at 37°C (5% CO₂)
10 diluted in conditioned medium from SMLC. Fluorescently labelled immune cells were allowed to
11 accumulate on the EECM-BMEC-like cell monolayer at a low flow rate of 0.1 dyne/cm² for 4 min, and
12 then the flow rate was set to the physiological level of 1.5 dyne/cm² for 16 min (shear phase). The
13 dynamic immune cell interactions with the EECM-BMEC-like cell monolayers under the physiological
14 flow were recorded with a Zeiss AxioCam MRm camera. Immune cell behavior on the EECM-BMEC-like
15 cell monolayer was categorized as described previously.⁴⁵ In brief, Th1* cells and PBMCs found to
16 polarize upon arrest and to migrate across the EECM-BMEC-like cells monolayer with or without prior
17 crawling or probing on the EECM-BMEC-like cells were categorized as “diapedesis”. Th1* cells and
18 PBMCs that crawled on the surface of the EECM-BMEC-like cells for the entire observation time were
19 categorized as “crawling”. Th1* cells and PBMCs that remained stationary without displacing beyond a
20 distance exceeding their own diameter and presenting dynamic cellular protrusions were categorized as
21 “probing”.

22 **Quantitative RT-PCR**

23 RNA was isolated using High Pure RNA isolation kit (Roche) as instructed by the manufacturer, from
24 EECM-BMEC-like cells. For quantitative real time-polymerase chain reaction (PCR) analyses, total RNA
25 was reverse transcribed with Maxima H Minus cDNA Synthesis Master Mix (ThermoFisher Scientific),
26 and amplification was performed on an ABI PRISM 7000 Sequence Detection System (ThermoFisher
27 Scientific) using Takyon ROX SYBR Green MasterMix dTTP Blue (Eutogentec). Primer sequences are
28 reported in Supplementary Table 3. The relative expression of each mRNA was calculated by the
29 comparative threshold cycle method and normalized to β -actin mRNA expression.

30

1 **Statistical analysis**

2 Statistical analysis of the data was performed by the Clinical Trial Unit (CTU) of the University of Bern.
3 Multiple measurements per clone within each individual were analysed through a linear mixed model. In
4 order to take into account the potential correlation between clones from the same individual, random
5 intercept and slope for clone nested into individual were considered. Robust standard errors were
6 considered for the mixed model. Variances of the random parameters were displayed as well as the
7 intra-class correlation (ICC) between clones. The linear mixed model does not request for normal
8 distribution of the data but of the error terms of the model and there is no evidence against non-
9 normality of the errors in our dataset. Importantly, robust standard error is more stable against such
10 deviation and has been considered in our analysis. All analyses were done using Stata version 17.
11 StataCorp. 2021. Stata Statistical Software: Release 17. College Station, TX: StataCorp LLC. p-values are
12 indicated in each figure.

13 **Study approval**

14 All subjects have given their written informed consent for establishing hiPSCs (consent form 107/13 and
15 2018-01622 (MS 3 and MS4) and OFSEP consent (MS1 and MS2)) and derivatives thereof according to
16 the ethical approval for the project entitled "COOLIN' BRAIN" given of the Cantonal Ethic Committee of
17 the Canton Vaud (Switzerland) (consent form 2018-01622).

18 **Data availability**

19 All data are available in the main text or the supplementary materials.

20 **Results**

21 **MS-derived Defined Medium Method (DMM)-BMEC-like cells show impaired barrier characteristics**

22 To investigate if BMEC-like cells differentiated from hiPSCs of MS patients model BBB dysfunction, we
23 established 6 hiPSC clones from 3 HCs and 7 hiPSC clones from 4 MS patients and differentiated them
24 into BMEC-like cells by the well-established and widely used Defined Medium Method (DMM).²³ BMEC-
25 like cells derived using the DMM method are particularly useful for the investigation of barrier and
26 transport characteristics of the human BBB, despite their shortcomings in modeling endothelial
27 development and immune cell interactions.^{20,46-48} We found that both HC- and MS-derived DMM-BMEC-
28 like cells show junctional localization of the tight junction molecules claudin-5 and occludin and the
29 junctional scaffolding protein ZO-1 (Figure 1A). However, MS-derived DMM-BMEC-like cells were larger

1 in size when compared to HC-derived DMM-BMEC-like cells despite equivalent seeding densities two
2 days prior to analysis (Figure 1A). When investigating barrier characteristics of DMM-BMEC-like cells by
3 studying the transendothelial electrical resistance (TEER) and the permeability to the small molecule
4 tracer sodium fluorescein (NaFl, 0.37 kDa), we found that MS-derived DMM-BMEC-like cells showed an
5 accelerated decline of TEER (Figure 1B) and a significantly higher permeability to NaFl (Figure 1C) when
6 compared to HC-derived DMM-BMEC-like cells. Thus, MS-derived DMM-BMEC-like cells display a
7 distinct morphology with impaired junctional integrity and barrier characteristics when compared to HC-
8 derived DMM-BMEC-like cells.

9 **MS-derived DMM-BMEC-like cells display reduced P-glycoprotein efflux pump activity**

10 As expression of the efflux pump P-glycoprotein (P-gp) is known to be reduced in active MS lesions and
11 P-gp function is impaired in EAE¹⁴ we next asked if any changes in P-gp activity could be detected in MS-
12 derived DMM-BMEC-like cells. To this end, we assessed the accumulation of the P-gp substrate
13 Rhodamine 123 in the presence or absence of the P-gp inhibitor cyclosporin (CsA) in MS- and HC-derived
14 DMM-BMEC-like cells. While we observed increased accumulation of Rhodamine 123 in both MS- and
15 HC-derived DMM-BMEC-like cells upon CSA treatment, accumulation of Rhodamine 123 was
16 significantly lower in MS-derived DMM-BMEC-like cells compared to HC-derived DMM-BMEC-like cells
17 (Figure 1D, HC: 172.7±26.63 %, MS: 123.7±19.27 %), indicating an impaired P-gp function.

18 **MS-derived DMM-BMEC-like cells show increased cell surface staining of ICAM-1**

19 Another key pathological hallmark of MS is increased expression of endothelial adhesion molecules
20 mediating CNS immune cell infiltration. Therefore, we next asked if MS-derived DMM-BMEC-like cells
21 show increased cell surface expression of ICAM-1, which mediates T-cell arrest and crawling on the
22 inflamed BBB.⁴⁹ Comparing cell surface expression of ICAM-1 by flow cytometry, we found that both HC-
23 and MS-derived DMM-BMEC-like cells stained positive for ICAM-1, and proinflammatory cytokine
24 stimulation induced further upregulation of ICAM-1. Interestingly, MS-derived DMM-BMEC-like cells
25 showed a significantly higher cell surface ICAM-1 staining under both non-stimulated and
26 proinflammatory cytokine-stimulated conditions compared to HC-derived DMM-BMEC-like cells (Figures
27 1E and 1F). Increased ICAM-1 expression on MS-derived DMM-BMEC-like cells suggests an intrinsic
28 inflammatory phenotype that may contribute to increased immune cell trafficking into the CNS in MS.

29 **EECM-BMEC-like cells from MS patients show disrupted tight junctions and impaired barrier** 30 **properties**

31 As DMM-BMEC-like cells do not express other key adhesion molecules expressed on the BBB *in vivo*,²⁰
32 they are not suited to model BBB-immune cell interactions in MS. We therefore conducted further
33 studies using a complementary hiPSC BBB model known as EECM-BMEC-like cells, which we have
34 previously shown to be suitable to study immune cell interactions with the BBB *in vitro*.²⁰ Therefore, we
35 differentiated 6 hiPSC clones from 3 HCs and 7 hiPSC clones from 4 MS patients into BMEC-like cells by
36 EECM. We first asked whether the observed MS-associated BBB dysfunction modeled by DMM-BMEC-
37 like cells could be reproduced with EECM-BMEC-like cells. We successfully differentiated HC- and MS-
38 derived iPSCs to EECM-BMEC-like cells that showed junctional localization of adherens and tight junction

1 proteins VE-cadherin, claudin-5 and occludin (Figure 2A). We have previously shown that EECM-BMEC-
2 like cells have a morphology that is distinct from DMM-BMEC-like cells and resembles more that of
3 primary brain microvascular endothelial cells^{20,43}. In accordance with observations of DMM-BMEC-like
4 cells, MS-derived EECM-BMEC-like cells were larger in size (Supplementary Figure 1) and showed
5 interrupted junctional staining for the tight junction proteins claudin-5 and occludin despite equal
6 seeding density (Figure 2A). MS-derived EECM-BMEC-like cells established a significantly lower TEER and
7 showed a significantly increased permeability to NaFl when compared to HC-derived EECM-BMEC-like
8 cells (Figures 2B, 2C, 2D). Importantly, we previously demonstrated that co-culture of EECM-BMEC-like
9 cells with SMLC derived from the same hiPSC clones helped to improve the adhesion molecule
10 repertoire.²⁰ Co-culture with SMLC increased permeability in both HC and MS-derived EECM-BMEC-like
11 cells, with MS-derived EECM-BMEC-like cells having a similar fold increased in permeability as in the
12 monoculture case. (Figure 2E). To investigate the possibility that larger morphology, interrupted tight
13 junction proteins and corresponding impairment of barrier properties of MS-derived EECM-BMEC-like
14 cells was caused by a slower proliferation rate, we cultured MS-derived EECM-BMEC-like cells for 8 days
15 (2 days longer) after seeding on the Transwell filter and evaluated claudin-5 staining by
16 immunocytochemistry. The morphology and interrupted claudin-5 staining of MS-derived EECM-BMEC-
17 like cells were unchanged (Supplementary Figure 1A). We also investigated the permeability of NaFl in
18 HC- vs MS-derived EECM-BMEC-like cell monolayers at different seeding densities, lower density for HC
19 and higher density for MS. Although HC-derived EECM-BMEC-like cells in monolayers obtained from
20 reduced seeding density displayed a morphology comparable to that of MS-derived EECM-BMEC-like
21 cells at normal density, they sustained continuous junctional localization of claudin-5 and low
22 permeability to NaFl (Supplementary Figure 1). Also, MS-derived EECM-BMEC-like cell monolayers
23 obtained after increased EECM-BMEC-like cell seeding density did not show any difference in
24 permeability for NaFl when compared to regular seeding density (Supplementary Figure 1B, 1C, 1D).
25 These results indicate that while cellular morphology is dependent on seeding density, impaired
26 functionality of MS-derived EECM-BMEC-like cells does not depend on seeding densities. Thus, MS-
27 derived EECM-BMEC-like cells show impaired junctional integrity and defective barrier properties
28 suggesting that BBB dysfunction in MS can indeed be modeled with hiPSC-derived EECM-BMEC-like cells.

29 **MS-derived EECM-BMEC-like cells show increased cell surface staining of ICAM-1 and VCAM-1**

30 We next asked if using EECM-BMEC-like cells we could also model increased expression of ICAM-1 and
31 VCAM-1 as observed in brain endothelium of MS patients.⁵⁰ To this end, we immunolabeled for
32 endothelial adhesion molecules ICAM-1 and VCAM-1 on EECM-BMEC-like cells co-cultured with SMLCs
33 (Figure 3A). We found that MS-derived EECM-BMEC-like cells had a qualitatively higher ICAM-1 signal
34 under both non-stimulated and proinflammatory cytokine-stimulated (1 ng/mL TNF- α + 20 IU/mL IFN- γ)
35 conditions and higher VCAM-1 signal under proinflammatory cytokine-stimulated conditions compared
36 to HC-derived EECM-BMEC-like cells (Figure 3A). Quantitative flow cytometry analyses of non-stimulated
37 (NS) or proinflammatory cytokine-stimulated EECM-BMEC-like cells confirmed the increased cell surface
38 expression of ICAM-1 and VCAM-1 in MS-derived EECM-BMEC-like cells (Figure 3B and 3C). Mean
39 fluorescence intensities for VCAM-1 seemed generally much lower when compared to ICAM-1 (Figure
40 3C) and were accordingly barely detectable by immunofluorescence staining on non-stimulated EECM-

1 BMEC-like cells (Figure 3A). Finally, when comparing the fold upregulation of ICAM-1 and VCAM-1 after
2 cytokine stimulation, HC-derived and MS-derived EECM-BMEC-like cells did not show any difference
3 (data not show). Taken together, MS-derived EECM-BMEC-like cells displayed significantly increased
4 expression of ICAM-1 at both basal and cytokine-stimulated conditions and VCAM-1 at basal condition
5 and thus permit modeling of the inflammatory BBB phenotype observed in MS *in vivo*.

6 **MS-derived EECM-BMEC-like cells promote increased adhesion and transmigration of allogeneic Th1*** 7 **cells**

8 As we have previously shown that ICAM-1 and VCAM-1 on EECM-BMEC like cells mediate T-cell
9 adhesion,²⁰ we next asked if increased expression of ICAM-1 and VCAM-1 in MS-derived EECM-BMEC-
10 like cells would translate to increased T cell trafficking across their barrier. To this end, we first
11 investigated the interaction of EECM-BMEC-like cells with Th1* cells since this T cell subset is present in
12 CSF and brain parenchyma of MS patients^{51,52} and thought to contribute to MS pathogenesis because of
13 its mixed Th1/Th17 signature cytokine profile secreting IFN- γ , IL-17 and GM-CSF.⁵¹⁻⁵³ Incubating
14 allogeneic Th1* cells isolated from healthy donors with MS-derived and HC-derived EECM-BMEC-like cell
15 monolayers under static conditions (Figure 4A) we found an increased tendency in adhesion of Th1*
16 cells to MS-derived EECM-BMEC-like cells when compared to HC-derived EECM-BMEC-like cells under
17 non-stimulated but no longer under cytokine-stimulated conditions, when adhesion molecule
18 expression on HC-EECM-BMEC-like cells was further upregulated (Figure 4B). To determine if increased
19 interaction of Th1* cells with MS-derived EECM-BMEC-like cells would also lead to increased Th1* cell
20 migration across MS-derived EECM-BMEC-like cells, we next investigated the interaction of Th1* cells
21 with EECM-BMEC-like cells under physiological flow by *in vitro* live cell imaging (Figure 4C). Under these
22 conditions, which better recapitulate the sequential adhesive interactions of the multi-step T-cell
23 extravasation cascade as they occur *in vivo*, we could observe increased shear resistant arrest of
24 allogeneic Th1* cells to cytokine-stimulated MS-derived EECM-BMEC-like cells when compared to HC-
25 derived EECM-BMEC-like cells (Figure 4D). This ultimately translated into increased Th1* cell diapedesis
26 across MS-derived EECM-BMEC-like cells compared to HC-derived EECM BMEC-like cells (Figure 4D, and
27 Supplementary Movies 1 and 2). Upon shear resistant arrest, T cells either probe the endothelial cell
28 surface by sending out cellular protrusions or they crawl over the endothelial surface to find sites
29 permissive for diapedesis.⁴⁹ The majority of Th1* cells crossed the EECM-BMEC-like cell monolayers
30 after probing while a lower percentage crossed the EECM-BMEC-like cell monolayers after crawling
31 (Figure 4E). The percentage of arrested Th1* cells that crossed the EECM-BMEC-like cells after probing
32 was significantly higher in MS-derived EECM-BMEC-like cells compared to HC-derived EECM-BMEC-like
33 cells. Conversely, Th1* cell probing or crawling on the EECM-BMEC-like cell surface over the entire assay
34 period without diapedesis was significantly higher on HC-EECM-BMEC-like cells when compared to their
35 MS counterparts suggesting that lower cell surface expression of adhesion molecules on HC-EECM-
36 BMEC-like cells delayed the Th1* cells in finding appropriate sites for diapedesis (Figure 4E). Taken
37 together, these observations underscore that alterations in MS-derived EECM-BMEC-like cells cause
38 increased T-cell adhesion followed by increased T-cell diapedesis as compared to HC-derived EECM-
39 BMEC-like cells reflecting the observations made *in vivo* in MS.

40

1 **MS-derived EECM-BMEC-like cells support increased interaction with autologous PBMCs**

2 Having established that MS-derived EECM-BMEC like cells model BBB impairment and an increased
3 inflammatory phenotype as observed in MS *in vivo* we made use of this unprecedented opportunity to
4 study MS-patient derived immune cell interactions with the BBB in an entirely autologous fashion *in*
5 *vitro*. To this end we obtained PBMCs from HC2 and MS3 and compared their interactions side-by-side
6 with HC2- and MS3-derived EECM-BMEC like-cells in an autologous or heterologous setting under
7 physiological flow by *in vitro* live cell imaging. Although we showed in a previous study that DMF
8 reduces binding of peripheral blood T cells to the BBB *in vitro*⁵⁴, when comparing the autologous
9 interactions of PBMCs with EECM-BMEC-like cells we here found significantly higher numbers of MS3-
10 derived PBMCs adhering to or crossing MS3-derived EECM-BMEC-like cell monolayers when compared
11 to HC2-PBMCs interaction with HC2-derived EECM-BMEC-like cells (Figure 4F). In depth analysis of the
12 individual post-arrest behavior of PBMCs on the EECM-BMEC-like cell monolayers showed that in the
13 autologous MS system, there was a trend towards increased diapedesis in both probing and crawling
14 PBMCs accompanied by a trend towards reduced PBMC detachment (Figure 4G). However, as the
15 composition and activation stage of PBMCs in MS patients differs from that in HCs we next asked if
16 increased interaction of PBMCs with EECM-BMEC-like cells as observed in the autologous MS setting is
17 truly a function of the BMEC-like cells themselves. To this end, we analyzed the interaction of HC2-
18 derived PBMCs with MS3-derived EECM-BMEC-like cells and MS3-derived PBMCs with HC2-derived
19 EECM-BMEC-like cells under physiological flow *in vitro*. MS3-derived EECM-BMEC-like cells supported a
20 significantly increased arrest, crawling and diapedesis of HC2-derived PBMCs under physiological flow *in*
21 *vitro* when compared to the autologous HC2-derived EECM-BMEC-like cells (Supplementary Figure 2A
22 and 2B). Also, MS3 PBMCs showed a significantly increased arrest and subsequent probing on
23 autologous EECM-BMEC-like cells when compared to HC2-derived EECM-BMEC-like cells (Supplementary
24 Figure 2C and 2D). Taken together these data underscore the inflammatory phenotype and active role of
25 the MS-derived EECM-BMEC-like cells in increasing immune cell entry into the CNS and their suitability
26 to explore immune functions of the BBB in an entirely autologous fashion.

27 **Activation of Wnt/ β -catenin signaling restores barrier properties of MS-derived EECM-BMEC-like cells**

28 Having established that MS-derived EECM-BMEC-like cells are suitable to model BBB dysfunction in MS
29 we next explored if this model is appropriate to evaluate therapeutic strategies for the treatment of MS
30 at the level of the BBB. As the canonical Wnt/ β -catenin signaling pathway is involved in BBB
31 development and maintenance,⁵⁵⁻⁵⁷ and we have demonstrated that activation of Wnt/ β -catenin
32 signaling upregulates claudin-5 and induced other BBB properties in hPSC-derived generic ECs,⁵⁸ we
33 investigated if expression of molecules involved in canonical Wnt/ β -catenin signaling is modulated in
34 MS-derived EECM-BMEC-like cells. To this end we performed RT-qPCR experiments (Supplementary
35 Figure 3 A-E). While *FZD3*, *FZD4* and *LEF1* mRNA expression were not modified, we found mRNA
36 expression of the canonical wnt-target gene *AXIN2* to be significantly decreased and mRNA expression
37 of *FZD6*, previously reported as negative regulator of wnt-signaling to be significantly increased⁵⁹ in MS-
38 derived EECM-BMEC-like cells compared to HC-derived EECM-BMEC-like cells. These data indicate that
39 canonical Wnt/ β -catenin signaling is impaired in MS-derived EECM-BMEC-like cells. Therefore, we next
40 asked if activation of Wnt/ β -catenin signaling in MS-derived EECM-BMEC-like cells would improve their

1 barrier function. To this end, we cultured endothelial progenitor cells (EPCs) in the presence or absence
2 of the GSK-3 inhibitor, CHIR99021, to activate Wnt/ β -catenin signaling until they reached passage 3
3 (Figure 5A). We investigated subcellular localization of claudin-5 in EECM-BMEC-like cells since
4 junctional localization of claudin-5 correlates to BBB integrity in humans *in vivo* and is a known target of
5 Wnt signaling.⁶⁰ Activation of canonical Wnt/ β -catenin signaling in MS-derived EPCs resulted in
6 improved junctional localization of claudin-5 and occludin in differentiated EECM-BMEC-like cells (Figure
7 5B, Supplementary figure 3). This was accompanied by reduced permeability of CHIR99021-pretreated
8 EECM-BMEC-like cells to sodium fluorescein, reaching permeability levels comparable to HC-derived
9 EECM-BMEC-like cells (Figure 5C and Figure 2D, MS-derived EECM-BMEC-like cells from EPCs treated
10 with CHIR99021 $0.147 \pm 0.081 \times 10^{-3}$ cm/min vs HC-derived EECM-BMEC-like cells $0.208 \pm 0.058 \times 10^{-3}$
11 cm/min). We furthermore observed that activation of Wnt/ β -catenin signaling in MS-derived EPCs
12 reduced cell surface expression of VCAM-1, but not ICAM-1 in cytokine-stimulated MS-derived EECM-
13 BMEC-like cells (Figure 5D and E). Thus, activation of Wnt/ β -catenin signaling during the differentiation
14 of MS-derived EECM-BMEC-like cells could restore barrier properties and reduce the inflammatory
15 phenotype, underscoring the suitability of MS-derived EECM-BMEC-like cells for exploring therapeutic
16 avenues for BBB stabilization and inhibition of CNS inflammation.

17 Discussion

18 The establishment of patient-sourced hiPSC-derived BMEC-like cells as *in vitro* model for the BBB has
19 paved the way to study BBB dysfunction in a personalized fashion by providing a scalable and renewable
20 source of BMECs from one individual. Human iPSC-derived *in vitro* models of the BBB have been
21 established using different differentiation protocols^{19,20,22,23,43} and have already proven successful to
22 model BBB dysfunction in inheritable neurological disorders like Huntington's disease, familial
23 Parkinson's disease, familial amyotrophic lateral sclerosis (ALS), familial Alzheimer's disease, and MCT8
24 deficiency *in vitro*.^{24,25,27} Previous studies making use of hiPSCs from patients with sporadic ALS have
25 proven suitable for exploring disease pathogenesis.⁶¹ This encouraged us to establish hiPSCs from MS
26 patients and healthy controls to explore if intrinsic defects in brain endothelial cells contribute to BBB
27 dysfunction in MS, which may thus reveal a pathogenic process not yet fully understood.
28 BBB dysfunction accompanied by increased immune cell infiltration into the CNS is an early hallmark of
29 MS pathogenesis and BBB dysfunction detected as Gd-enhancing lesions by MRI is one of the diagnostic
30 criteria for MS. The etiology of MS remains unknown. However, given recent discoveries that MS-
31 associated genetic variants code for molecules related to the function of specific immune cell subsets,
32 the disease is considered a chronic inflammatory CNS disease of autoimmune etiology, influenced by
33 genetic and environmental factors.⁶² Immune cells from blood or CSF of MS patients have thus been
34 extensively studied, which has increased our understanding of MS pathogenesis, leading to current
35 development of immunomodulatory therapies for preventing MS relapse. The individual differences
36 observed in response to MS immunomodulatory therapies combined with the variable disease course
37 underscore that the underlying pathogenesis in MS may be much more complex than presently thought.

1 To this end, the GWAS studies in MS have provided little evidence for a causal contribution of CNS-
2 resident cells in MS pathogenesis. However this may change with increasing availability of CNS datasets
3 pointing to the contribution of CNS-resident cells in MS pathogenesis.⁶³ Therefore, there is an unmet
4 need for continued detailed phenotypic and functional analysis of disease-relevant tissues directly
5 derived from MS patients to unravel the etiology of MS in its entire complexity.

6 In this study, we show that MS-derived hiPSC-derived BMEC-like cells model BBB alterations in MS *in*
7 *vitro*. Comparing MS- versus HC-derived BMEC-like cells we found that MS-derived BMEC-like cells
8 displayed reduced barrier characteristics shown by impaired junctional integrity, reduced TEER,
9 increased permeability to small molecular tracers and impaired efflux pump activity. These phenotypes
10 are reflective of reports of BBB dysfunction observed in rodent models and humans.^{8-11,14-16,64,65}
11 Importantly, barrier dysfunction in MS-derived BMEC-like cells was observed using two distinct
12 differentiation protocols, namely DMM²³ and EECM^{20,43} and in BMEC-like cells from multiple hiPSC
13 clones. Although biological sample size in our study is still limited, the observation that all MS-derived
14 BMEC-like cells display altered barrier properties when compared to HC-derived BMEC-like cells
15 highlights that the impaired barrier characteristics observed in MS-derived BMEC-like cells are really
16 intrinsic to MS and are likely a result of the genetic or epigenetic profile of each individual rather than a
17 methodological artifact. These data thus strongly support that MS patients have intrinsic alterations in
18 their brain endothelium that lead to BBB dysfunction, which can be modeled by hiPSC-derived BMEC-
19 like cells.

20 Making use of the EECM-BMEC-like cells, we further showed that impaired barrier characteristics of MS-
21 derived BMEC-like cells were accompanied by a pro-inflammatory phenotype characterized by enhanced
22 expression of VCAM-1 and ICAM-1 and increased immune cell interactions under static and physiological
23 flow conditions. Making use of MS-patient derived *in vitro* BBB models, we had the unprecedented
24 opportunity to explore how this altered BBB phenotype affects immune cell interaction in an entirely
25 autologous fashion. Our observations underscore the active role of MS-derived EECM-BMEC-like cells in
26 mediating the increased interaction of autologous PBMCs under static and physiological flow conditions
27 leading to their enhanced migration across BMEC-like cells *in vitro*. MS-derived EECM-BMEC-like cells
28 are thus a suitable model to study the molecular mechanisms leading to increased immune cell
29 infiltration into the CNS during MS in an autologous fashion.

30 Having established that MS-derived BMEC-like cells allow modeling of BBB dysfunction observed in MS,
31 we next asked if these hiPSC-derived *in vitro* BBB models are suitable to explore therapeutic approaches
32 for restoring BBB function as potential novel treatment strategy in MS. Based on the observation that
33 endothelial Wnt/ β -catenin signaling is involved in BBB development and maturation, where Wnt/ β -
34 catenin signaling pathway stabilizes endothelial adherens junctions and tight junctions,^{55-57,66,67} we asked
35 if triggering the Wnt/ β -catenin signaling pathway in MS-derived EECM-BMEC-like cells would restore
36 barrier function. We indeed observed that activation of the Wnt/ β -catenin signaling pathway in MS-
37 derived EECM-BMEC like cells restored their junctional integrity by improving junctional localization of
38 claudin-5 as well as their barrier properties making them comparable to HC-derived EECM-BMEC-like
39 cells. Our observations thus suggest that activation of the Wnt/ β -catenin signaling pathway in brain
40 endothelial cells may allow restoration of BBB function in MS. Activation of endothelial Wnt/ β -catenin
41 signaling has proven beneficial in animal models of stroke.^{68,69} In the case of MS, the Wnt/ β -catenin

1 pathway was reported to be up-regulated in brain endothelial cells in MS and in the mouse model
2 experimental autoimmune encephalomyelitis (EAE),⁷⁰ where its increased activity in brain endothelial
3 cells during EAE progression was found to correlate to breakdown of the endothelial cell junctions,
4 suggesting upregulation of Wnt/ β -catenin pathway for restoring BBB function. It thus remains to be
5 shown if the presence of pro-inflammatory factors inducing BBB dysfunction *in vivo*^{62,71-76} may mask the
6 effect of Wnt/ β -catenin signaling in stabilizing BBB junctions.

7 In accordance with the observations in EAE *in vivo*,⁷⁰ we also observed that activation of Wnt/ β -catenin
8 signaling in MS-derived EPCs induced a quiescent immune phenotype in MS-EECM-BMEC-like cells with
9 reduced expression of VCAM-1 that may result in reduced immune cell interaction. Taken together,
10 these findings suggest that activation of endothelial Wnt/ β -catenin signaling is a promising approach to
11 restore barrier properties and a quiescent immune phenotype of the BBB in MS.

12 These findings are especially relevant given the fact that the current immunomodulatory treatments in
13 MS mainly target immune cells and have limited effects on the progressive phase of MS. Therapeutic
14 stabilization of impaired BBB function by activating Wnt/ β -catenin signaling in brain endothelial cells or
15 by other methods may thus open up entirely novel avenues for therapeutic intervention in MS by re-
16 establishing CNS homeostasis and preventing disease progression. Consistent with this hypothesis,
17 ectopic endothelial cell-specific expression of the tight junction sealing protein claudin-1 reduced BBB
18 leakiness to plasma proteins during EAE resulting in amelioration of the chronic phase of the disease.⁷⁷

19 Our observations thus suggests that hiPSC-derived BMEC-like cells from MS patients, and especially
20 EECM-BMEC-like cells, model BBB dysfunction in MS with respect to junctional integrity, diffusion
21 barrier properties, efflux pump activity, adhesion molecule phenotype, and autologous immune cell
22 interaction. However, a shortcoming of our current study is that the matching of the MS patients and
23 HC especially with respect to age was not ideal with the HC individuals being older than the MS patients.
24 However, if age played a major role in determining the barrier properties of the hiPSC-derived BMEC-like
25 cells we would have rather expected to see impaired barrier properties and an inflammatory phenotype
26 in EECM-BMEC-like cells derived from hiPSC from the older individuals as BBB impairment is observed in
27 healthy ageing⁷⁸. The observation that EECM-BMEC-like cells derived from the younger MS patients
28 displayed impaired barrier properties and an inflammatory phenotype when compared to those from
29 the older HC-derived EECM-BMEC-like cells suggests that it is the condition of MS rather than the age of
30 the individuals that correlates with impaired BBB properties.

31 Taken together, we consider hiPSC-derived BMEC-like cells to provide an unprecedented opportunity to
32 explore the molecular mechanisms underlying BBB dysfunction in MS. Future studies comparing a higher
33 number of sex and age matched HC and MS-patients and combining characterization of the
34 transcriptional, phenotypic and functional profile of MS-derived EECM-BMEC-like cells compared to
35 their HC counterparts will be necessary to identify the potential BBB dysfunction gene signatures in MS.
36 This will set the stage for designing entirely novel therapeutic approaches that aim to stabilize BBB
37 function in MS, bearing the hope of delaying disease onset, improving neuroprotection and preventing
38 secondary progressive MS.

39

1 **Acknowledgements**

2 We thank David Laplaud for providing blood samples from two MS subjects enrolled in this study.

3 **Funding**

4 This study was funded by the SNSF (grant N° 310030_189080), the Bangerter-Rhyner
5 Foundation and the Bern Center for Precision Medicine to BE, the Swiss MS Society to BE and
6 RDP; anECTRIMS Postdoctoral Research Exchange Fellowship, the Uehara Memorial
7 Foundation, and JSPS Overseas Research Fellowships, and FOCS project of Yamaguchi
8 University to HN, and National Institutes of Health Grant NS103844 to EVS and SPP. RDP was
9 also supported by a SNSF 320030-179531. BDG was supported by the National Science
10 Foundation Graduate Research Fellowship program under grant number 1747503 and the
11 National Institutes of Health Biotechnology Training Program grant T32 GM008349.

12 **Competing interests**

13 BE received a grant from Biogen to study extended dosing of Natalizumab on T-cell migration across the
14 blood-brain barrier and a grant from CSL Behring to investigate the molecular underpinnings of blood-
15 brain barrier dysfunction in neurological disorders. HN, BDG, SPP, EVS, and BE are inventors on
16 provisional US patent applications related to the EECM-BMEC-like cells (63/084980 and 63/185815).

17 **Supplementary material**

18 Supplementary material is available at *Brain* online.

1 References

- 2 1. Axisa PP, Hafler DA. Multiple sclerosis: genetics, biomarkers, treatments. *Current*
3 *opinion in neurology*. Jun 2016;29(3):345-53. doi:10.1097/wco.0000000000000319
- 4 2. Consortium IMSG. Low-Frequency and Rare-Coding Variation Contributes to Multiple
5 Sclerosis Risk. *Cell*. Nov 29 2018;175(6):1679-1687.e7. doi:10.1016/j.cell.2018.09.049
- 6 3. Thompson AJ, Baranzini SE, Geurts J, Hemmer B, Ciccarelli O. Multiple sclerosis.
7 *Lancet*. Apr 21 2018;391(10130):1622-1636. doi:10.1016/s0140-6736(18)30481-1
- 8 4. Kermode AG, Thompson AJ, Tofts P, et al. Breakdown of the blood-brain barrier
9 precedes symptoms and other MRI signs of new lesions in multiple sclerosis. Pathogenetic and
10 clinical implications. *Brain : a journal of neurology*. Oct 1990;113 (Pt 5):1477-89.
- 11 5. Filippi M, Rovaris M, Capra R, et al. A multi-centre longitudinal study comparing the
12 sensitivity of monthly MRI after standard and triple dose gadolinium-DTPA for monitoring
13 disease activity in multiple sclerosis. Implications for phase II clinical trials. *Brain : a journal of*
14 *neurology*. Oct 1998;121 (Pt 10):2011-20. doi:10.1093/brain/121.10.2011
- 15 6. Werring DJ, Brassat D, Droogan AG, et al. The pathogenesis of lesions and normal-
16 appearing white matter changes in multiple sclerosis: a serial diffusion MRI study. *Brain : a*
17 *journal of neurology*. Aug 2000;123 (Pt 8):1667-76. doi:10.1093/brain/123.8.1667
- 18 7. Goodkin DE, Rooney WD, Sloan R, et al. A serial study of new MS lesions and the white
19 matter from which they arise. *Neurology*. Dec 1998;51(6):1689-97. doi:10.1212/wnl.51.6.1689
- 20 8. Plumb J, McQuaid S, Mirakhur M, Kirk J. Abnormal endothelial tight junctions in active
21 lesions and normal-appearing white matter in multiple sclerosis. *Brain pathology (Zurich,*
22 *Switzerland)*. Apr 2002;12(2):154-69.
- 23 9. Kirk J, Plumb J, Mirakhur M, McQuaid S. Tight junctional abnormality in multiple
24 sclerosis white matter affects all calibres of vessel and is associated with blood-brain barrier
25 leakage and active demyelination. *The Journal of pathology*. Oct 2003;201(2):319-27.
26 doi:10.1002/path.1434
- 27 10. Leech S, Kirk J, Plumb J, McQuaid S. Persistent endothelial abnormalities and blood-
28 brain barrier leak in primary and secondary progressive multiple sclerosis. *Neuropathology and*
29 *applied neurobiology*. Feb 2007;33(1):86-98. doi:10.1111/j.1365-2990.2006.00781.x
- 30 11. Alvarez JI, Cayrol R, Prat A. Disruption of central nervous system barriers in multiple
31 sclerosis. *Biochimica et biophysica acta*. Feb 2011;1812(2):252-64.
32 doi:10.1016/j.bbadis.2010.06.017
- 33 12. Alvarez JI, Saint-Laurent O, Godschalk A, et al. Focal disturbances in the blood-brain
34 barrier are associated with formation of neuroinflammatory lesions. *Neurobiology of disease*.
35 Feb 2015;74:14-24. doi:10.1016/j.nbd.2014.09.016
- 36 13. Vos CM, Geurts JJ, Montagne L, et al. Blood-brain barrier alterations in both focal and
37 diffuse abnormalities on postmortem MRI in multiple sclerosis. *Neurobiology of disease*. Dec
38 2005;20(3):953-60. doi:10.1016/j.nbd.2005.06.012
- 39 14. Kooij G, van Horssen J, de Lange EC, et al. T lymphocytes impair P-glycoprotein
40 function during neuroinflammation. *Journal of autoimmunity*. Jun 2010;34(4):416-25.
41 doi:10.1016/j.jaut.2009.10.006
- 42 15. Sobel RA, Mitchell ME, Fondren G. Intercellular adhesion molecule-1 (ICAM-1) in
43 cellular immune reactions in the human central nervous system. *The American journal of*
44 *pathology*. Jun 1990;136(6):1309-16.

- 1 16. Cayrol R, Wosik K, Berard JL, et al. Activated leukocyte cell adhesion molecule
2 promotes leukocyte trafficking into the central nervous system. *Nature immunology*. Feb
3 2008;9(2):137-45. doi:10.1038/ni1551
- 4 17. Minten C, Alt C, Gentner M, et al. DARC shuttles inflammatory chemokines across the
5 blood-brain barrier during autoimmune central nervous system inflammation. *Brain : a journal*
6 *of neurology*. May 2014;137(Pt 5):1454-69. doi:10.1093/brain/awu045
- 7 18. Klotz L, Kuzmanov I, Hucke S, et al. B7-H1 shapes T-cell-mediated brain endothelial
8 cell dysfunction and regional encephalitogenicity in spontaneous CNS autoimmunity.
9 *Proceedings of the National Academy of Sciences of the United States of America*. Oct 11
10 2016;113(41):E6182-E6191. doi:10.1073/pnas.1601350113
- 11 19. Lippmann ES, Azarin SM, Kay JE, et al. Derivation of blood-brain barrier endothelial
12 cells from human pluripotent stem cells. *Nature biotechnology*. Aug 2012;30(8):783-91.
13 doi:10.1038/nbt.2247
- 14 20. Nishihara H, Gastfriend BD, Soldati S, et al. Advancing human induced pluripotent stem
15 cell-derived blood-brain barrier models for studying immune cell interactions. *FASEB journal :*
16 *official publication of the Federation of American Societies for Experimental Biology*. Dec
17 2020;34(12):16693-16715. doi:10.1096/fj.202001507RR
- 18 21. Praca C, Rosa SC, Sevin E, Cecchelli R, Dehouck MP, Ferreira LS. Derivation of Brain
19 Capillary-like Endothelial Cells from Human Pluripotent Stem Cell-Derived Endothelial
20 Progenitor Cells. *Stem cell reports*. Sep 5 2019;13(4):599-611. doi:10.1016/j.stemcr.2019.08.002
- 21 22. Stebbins MJ, Wilson HK, Canfield SG, Qian T, Palecek SP, Shusta EV. Differentiation
22 and characterization of human pluripotent stem cell-derived brain microvascular endothelial
23 cells. *Methods (San Diego, Calif)*. May 15 2016;101:93-102. doi:10.1016/j.ymeth.2015.10.016
- 24 23. Qian T, Maguire SE, Canfield SG, et al. Directed differentiation of human pluripotent
25 stem cells to blood-brain barrier endothelial cells. *Science advances*. Nov 2017;3(11):e1701679.
26 doi:10.1126/sciadv.1701679
- 27 24. Lim RG, Quan C, Reyes-Ortiz AM, et al. Huntington's Disease iPSC-Derived Brain
28 Microvascular Endothelial Cells Reveal WNT-Mediated Angiogenic and Blood-Brain Barrier
29 Deficits. *Cell reports*. May 16 2017;19(7):1365-1377. doi:10.1016/j.celrep.2017.04.021
- 30 25. Vatine GD, Al-Ahmad A, Barriga BK, et al. Modeling Psychomotor Retardation using
31 iPSCs from MCT8-Deficient Patients Indicates a Prominent Role for the Blood-Brain Barrier.
32 *Cell stem cell*. Jun 01 2017;20(6):831-843.e5. doi:10.1016/j.stem.2017.04.002
- 33 26. Vatine GD, Barrile R, Workman MJ, et al. Human iPSC-Derived Blood-Brain Barrier
34 Chips Enable Disease Modeling and Personalized Medicine Applications. *Cell stem cell*. Jun 6
35 2019;24(6):995-1005.e6. doi:10.1016/j.stem.2019.05.011
- 36 27. Katt ME, Mayo LN, Ellis SE, et al. The role of mutations associated with familial
37 neurodegenerative disorders on blood-brain barrier function in an iPSC model. *Fluids and*
38 *barriers of the CNS*. Jul 15 2019;16(1):20. doi:10.1186/s12987-019-0139-4
- 39 28. Oikari LE, Pandit R, Stewart R, et al. Altered Brain Endothelial Cell Phenotype from a
40 Familial Alzheimer Mutation and Its Potential Implications for Amyloid Clearance and Drug
41 Delivery. *Stem cell reports*. May 12 2020;14(5):924-939. doi:10.1016/j.stemcr.2020.03.011
- 42 29. Nicaise AM, Banda E, Guzzo RM, et al. iPSC-derived neural progenitor cells from PPMS
43 patients reveal defect in myelin injury response. *Experimental neurology*. Feb 2017;288:114-
44 121. doi:10.1016/j.expneurol.2016.11.012

- 1 30. Song B, Sun G, Herszfeld D, et al. Neural differentiation of patient specific iPS cells as a
2 novel approach to study the pathophysiology of multiple sclerosis. *Stem cell research*. Mar
3 2012;8(2):259-73. doi:10.1016/j.scr.2011.12.001
- 4 31. Martínez-Larrosa J, Matute-Blanch C, Montalban X, Comabella M. Modelling multiple
5 sclerosis using induced pluripotent stem cells. *Journal of neuroimmunology*. Dec 15
6 2020;349:577425. doi:10.1016/j.jneuroim.2020.577425
- 7 32. Perriot S, Mathias A, Perriard G, et al. Human Induced Pluripotent Stem Cell-Derived
8 Astrocytes Are Differentially Activated by Multiple Sclerosis-Associated Cytokines. *Stem cell
9 reports*. Oct 12 2018;11(5):1199-1210. doi:10.1016/j.stemcr.2018.09.015
- 10 33. Douvaras P, Wang J, Zimmer M, et al. Efficient generation of myelinating
11 oligodendrocytes from primary progressive multiple sclerosis patients by induced pluripotent
12 stem cells. *Stem cell reports*. Aug 12 2014;3(2):250-9. doi:10.1016/j.stemcr.2014.06.012
- 13 34. García-León JA, Kumar M, Boon R, et al. SOX10 Single Transcription Factor-Based
14 Fast and Efficient Generation of Oligodendrocytes from Human Pluripotent Stem Cells. *Stem
15 cell reports*. Feb 13 2018;10(2):655-672. doi:10.1016/j.stemcr.2017.12.014
- 16 35. Ponath G, Lincoln MR, Levine-Ritterman M, et al. Enhanced astrocyte responses are
17 driven by a genetic risk allele associated with multiple sclerosis. *Nature communications*. Dec 17
18 2018;9(1):5337. doi:10.1038/s41467-018-07785-8
- 19 36. Nicaise AM, Wagstaff LJ, Willis CM, et al. Cellular senescence in progenitor cells
20 contributes to diminished remyelination potential in progressive multiple sclerosis. *Proceedings
21 of the National Academy of Sciences of the United States of America*. Apr 30
22 2019;116(18):9030-9039. doi:10.1073/pnas.1818348116
- 23 37. Morales Pantoja IE, Smith MD, Rajbhandari L, et al. iPSCs from people with MS can
24 differentiate into oligodendrocytes in a homeostatic but not an inflammatory milieu. *PloS one*.
25 2020;15(6):e0233980. doi:10.1371/journal.pone.0233980
- 26 38. Sullivan S, Stacey GN, Akazawa C, et al. Quality control guidelines for clinical-grade
27 human induced pluripotent stem cell lines. *Regen Med*. Oct 2018;13(7):859-866.
28 doi:10.2217/rme-2018-0095
- 29 39. Engen SA, Valen Rukke H, Becattini S, et al. The oral commensal *Streptococcus mitis*
30 shows a mixed memory Th cell signature that is similar to and cross-reactive with *Streptococcus
31 pneumoniae*. *PloS one*. 2014;9(8):e104306. doi:10.1371/journal.pone.0104306
- 32 40. Sallusto F, Schärli P, Loetscher P, et al. Rapid and coordinated switch in chemokine
33 receptor expression during dendritic cell maturation. *European journal of immunology*. Sep
34 1998;28(9):2760-9. doi:10.1002/(sici)1521-4141(199809)28:09<2760::Aid-
35 immu2760>3.0.Co;2-n
- 36 41. Wimmer I, Tietz S, Nishihara H, et al. PECAM-1 Stabilizes Blood-Brain Barrier Integrity
37 and Favors Paracellular T-Cell Diapedesis Across the Blood-Brain Barrier During
38 Neuroinflammation. Original Research. *Frontiers in immunology*. 2019-April-05
39 2019;10(711)doi:10.3389/fimmu.2019.00711
- 40 42. Jilek S, Schlupe M, Meylan P, et al. Strong EBV-specific CD8+ T-cell response in
41 patients with early multiple sclerosis. *Brain : a journal of neurology*. Jul 2008;131(Pt 7):1712-
42 21. doi:10.1093/brain/awn108
- 43 43. Nishihara H, Gastfriend BD, Kasap P, Palecek SP, Shusta EV, Engelhardt B.
44 Differentiation of human pluripotent stem cells to brain microvascular endothelial cell-like cells
45 suitable to study immune cell interactions. *STAR Protocols*. 2021;in press

- 1 44. Nishihara H, Soldati S, Mossu A, et al. Human CD4(+) T cell subsets differ in their
2 abilities to cross endothelial and epithelial brain barriers in vitro. *Fluids and barriers of the CNS*.
3 Feb 3 2020;17(1):3. doi:10.1186/s12987-019-0165-2
- 4 45. Mossu A, Rosito M, Khire T, et al. A silicon nanomembrane platform for the
5 visualization of immune cell trafficking across the human blood-brain barrier under flow.
6 *Journal of cerebral blood flow and metabolism : official journal of the International Society of*
7 *Cerebral Blood Flow and Metabolism*. Dec 19 2018;271678x18820584.
8 doi:10.1177/0271678x18820584
- 9 46. Workman MJ, Svendsen CN. Recent advances in human iPSC-derived models of the
10 blood-brain barrier. *Fluids and barriers of the CNS*. Apr 22 2020;17(1):30. doi:10.1186/s12987-
11 020-00191-7
- 12 47. Lippmann ES, Azarin SM, Palecek SP, Shusta EV. Commentary on human pluripotent
13 stem cell-based blood-brain barrier models. *Fluids and barriers of the CNS*. Oct 19
14 2020;17(1):64. doi:10.1186/s12987-020-00222-3
- 15 48. Lu TM, Houghton S, Magdeldin T, et al. Pluripotent stem cell-derived epithelium
16 misidentified as brain microvascular endothelium requires ETS factors to acquire vascular fate.
17 *Proceedings of the National Academy of Sciences of the United States of America*. Feb 23
18 2021;118(8)doi:10.1073/pnas.2016950118
- 19 49. Abadier M, Haghayegh Jahromi N, Cardoso Alves L, et al. Cell surface levels of
20 endothelial ICAM-1 influence the transcellular or paracellular T-cell diapedesis across the blood-
21 brain barrier. *European journal of immunology*. Apr 2015;45(4):1043-58.
22 doi:10.1002/eji.201445125
- 23 50. Nishihara H, Engelhardt B. Brain Barriers and Multiple Sclerosis: Novel Treatment
24 Approaches from a Brain Barriers Perspective. *Handbook of experimental pharmacology*. Nov
25 26 2020;doi:10.1007/164_2020_407
- 26 51. Kebir H, Ifergan I, Alvarez JI, et al. Preferential recruitment of interferon-gamma-
27 expressing TH17 cells in multiple sclerosis. *Annals of neurology*. Sep 2009;66(3):390-402.
28 doi:10.1002/ana.21748
- 29 52. van Langelaar J, van der Vuurst de Vries RM, Janssen M, et al. T helper 17.1 cells
30 associate with multiple sclerosis disease activity: perspectives for early intervention. *Brain : a*
31 *journal of neurology*. May 1 2018;141(5):1334-1349. doi:10.1093/brain/awy069
- 32 53. Jelcic I, Al Nimer F, Wang J, et al. Memory B Cells Activate Brain-Homing,
33 Autoreactive CD4(+) T Cells in Multiple Sclerosis. *Cell*. Sep 20 2018;175(1):85-100.e23.
34 doi:10.1016/j.cell.2018.08.011
- 35 54. Mathias A, Perriot S, Canales M, et al. Impaired T-cell migration to the CNS under
36 fingolimod and dimethyl fumarate. *Neurology(R) neuroimmunology & neuroinflammation*. Nov
37 2017;4(6):e401. doi:10.1212/nxi.0000000000000401
- 38 55. Zhou Y, Wang Y, Tischfield M, et al. Canonical WNT signaling components in vascular
39 development and barrier formation. *The Journal of clinical investigation*. Sep 2014;124(9):3825-
40 46. doi:10.1172/jci76431
- 41 56. Stenman JM, Rajagopal J, Carroll TJ, Ishibashi M, McMahon J, McMahon AP.
42 Canonical Wnt signaling regulates organ-specific assembly and differentiation of CNS
43 vasculature. *Science (New York, NY)*. Nov 21 2008;322(5905):1247-50.
44 doi:10.1126/science.1164594
- 45 57. Daneman R, Agalliu D, Zhou L, Kuhnert F, Kuo CJ, Barres BA. Wnt/beta-catenin
46 signaling is required for CNS, but not non-CNS, angiogenesis. *Proceedings of the National*

- 1 *Academy of Sciences of the United States of America*. Jan 13 2009;106(2):641-6.
2 doi:10.1073/pnas.0805165106
- 3 58. Gastfriend BD NH, Foreman KL, Engelhardt B, Palecek SP, Shusta EV. . Wnt signaling
4 mediates acquisition of blood-brain barrier properties in naïve endothelium derived from human
5 pluripotent stem cells. *eLife*. 2021;Nov 10;10:e70992.doi:10.7554/eLife.70992
- 6 59. Golan T, Yaniv A, Bafico A, Liu G, Gazit A. The human Frizzled 6 (HFz6) acts as a
7 negative regulator of the canonical Wnt. beta-catenin signaling cascade. *The Journal of*
8 *biological chemistry*. Apr 9 2004;279(15):14879-88. doi:10.1074/jbc.M306421200
- 9 60. Doherty CP, O'Keefe E, Wallace E, et al. Blood-Brain Barrier Dysfunction as a Hallmark
10 Pathology in Chronic Traumatic Encephalopathy. *Journal of neuropathology and experimental*
11 *neurology*. Jul 2016;75(7):656-62. doi:10.1093/jnen/nlw036
- 12 61. Fujimori K, Ishikawa M, Otomo A, et al. Modeling sporadic ALS in iPSC-derived motor
13 neurons identifies a potential therapeutic agent. *Nature medicine*. Oct 2018;24(10):1579-1589.
14 doi:10.1038/s41591-018-0140-5
- 15 62. Baecher-Allan C, Kaskow BJ, Weiner HL. Multiple Sclerosis: Mechanisms and
16 Immunotherapy. *Neuron*. Feb 21 2018;97(4):742-768. doi:10.1016/j.neuron.2018.01.021
- 17 63. Cotsapas C, Mitrovic M. Genome-wide association studies of multiple sclerosis. *Clinical*
18 *& translational immunology*. 2018;7(6):e1018. doi:10.1002/cti2.1018
- 19 64. Alvarez JI, Kebir H, Cheslow L, et al. JAML mediates monocyte and CD8 T cell
20 migration across the brain endothelium. *Annals of clinical and translational neurology*. Nov
21 2015;2(11):1032-7. doi:10.1002/acn3.255
- 22 65. Bennett J, Basivireddy J, Kollar A, et al. Blood-brain barrier disruption and enhanced
23 vascular permeability in the multiple sclerosis model EAE. *Journal of neuroimmunology*. Dec 15
24 2010;229(1-2):180-91. doi:10.1016/j.jneuroim.2010.08.011
- 25 66. Liebner S, Corada M, Bangsow T, et al. Wnt/beta-catenin signaling controls development
26 of the blood-brain barrier. *The Journal of cell biology*. Nov 3 2008;183(3):409-17.
27 doi:10.1083/jcb.200806024
- 28 67. Tran KA, Zhang X, Predescu D, et al. Endothelial β -Catenin Signaling Is Required for
29 Maintaining Adult Blood-Brain Barrier Integrity and Central Nervous System Homeostasis.
30 *Circulation*. Jan 12 2016;133(2):177-86. doi:10.1161/circulationaha.115.015982
- 31 68. Jean LeBlanc N, Menet R, Picard K, Parent G, Tremblay M, ElAli A. Canonical Wnt
32 Pathway Maintains Blood-Brain Barrier Integrity upon Ischemic Stroke and Its Activation
33 Ameliorates Tissue Plasminogen Activator Therapy. *Molecular neurobiology*. Sep
34 2019;56(9):6521-6538. doi:10.1007/s12035-019-1539-9
- 35 69. Song S, Huang H, Guan X, et al. Activation of endothelial Wnt/ β -catenin signaling by
36 protective astrocytes repairs BBB damage in ischemic stroke. *Progress in neurobiology*. Nov 26
37 2020:101963. doi:10.1016/j.pneurobio.2020.101963
- 38 70. Lengfeld JE, Lutz SE, Smith JR, et al. Endothelial Wnt/ β -catenin signaling reduces
39 immune cell infiltration in multiple sclerosis. *Proceedings of the National Academy of Sciences*
40 *of the United States of America*. Feb 14 2017;114(7):E1168-e1177.
41 doi:10.1073/pnas.1609905114
- 42 71. Hojati Z. Molecular Genetic and Epigenetic Basis of Multiple Sclerosis. *Advances in*
43 *experimental medicine and biology*. 2017;958:65-90. doi:10.1007/978-3-319-47861-6_6
- 44 72. Becher B, Spath S, Goverman J. Cytokine networks in neuroinflammation. *Nature*
45 *reviews Immunology*. Jan 2017;17(1):49-59. doi:10.1038/nri.2016.123

- 1 73. Brosnan CF, Cannella B, Battistini L, Raine CS. Cytokine localization in multiple
2 sclerosis lesions: correlation with adhesion molecule expression and reactive nitrogen species.
3 *Neurology*. Jun 1995;45(6 Suppl 6):S16-21.
- 4 74. Perriard G, Mathias A, Enz L, et al. Interleukin-22 is increased in multiple sclerosis
5 patients and targets astrocytes. *Journal of neuroinflammation*. Jun 16 2015;12:119.
6 doi:10.1186/s12974-015-0335-3
- 7 75. Yong VW, Zabad RK, Agrawal S, Goncalves Dasilva A, Metz LM. Elevation of matrix
8 metalloproteinases (MMPs) in multiple sclerosis and impact of immunomodulators. *Journal of*
9 *the neurological sciences*. Aug 15 2007;259(1-2):79-84. doi:10.1016/j.jns.2006.11.021
- 10 76. Kebir H, Kreymborg K, Ifergan I, et al. Human TH17 lymphocytes promote blood-brain
11 barrier disruption and central nervous system inflammation. *Nature medicine*. Oct
12 2007;13(10):1173-5. doi:10.1038/nm1651
- 13 77. Pfeiffer F, Schafer J, Lyck R, et al. Claudin-1 induced sealing of blood-brain barrier tight
14 junctions ameliorates chronic experimental autoimmune encephalomyelitis. *Acta*
15 *neuropathologica*. Nov 2011;122(5):601-14. doi:10.1007/s00401-011-0883-2
- 16 78. Montagne A, Barnes SR, Sweeney MD et al. Blood-brain barrier breakdown in the aging human
17 hippocampus. *Neuron*. Jan 2015;85(2):296-302.

18

ACCEPTED MANUSCRIPT

1 **Figure legends**

2 **Figure 1. Morphological and functional differences in MS-patient versus HC-derived DMM-BMEC-like** 3 **cells.**

4 **(A)** Representative stainings for ZO-1, claudin-5, or occludin (red), and nuclei (DAPI, blue) from HC1,
5 HC3, MS1, and MS4 are shown. Each staining is representative of at least 3 independent experiments
6 using 3 individual differentiations. Scale bar = 50 μ m. **(B)** Transendothelial electrical resistance (TEER)
7 measured with a Volt-Ohm-Meter. The black line represents mean \pm SD of 6 clones from 3 HC and red
8 line represents mean \pm SD of 7 clones from 4 MS patients each performed in triplicates and repeated at
9 least twice using 2 individual differentiations for each donor. **(C)** Permeability of sodium fluorescein
10 (NaFl) across DMM-BMEC-like cell monolayers was measured. **(D)** P-gp efflux pump activity was
11 assessed by intracellular accumulation of Rhodamine 123 in the presence or absence of the P-gp
12 inhibitor cyclosporine A (CsA). **(E)** Cell surface staining for the adhesion molecule ICAM-1 analyzed by
13 flow cytometry is shown. Isotype control, non-stimulated (NS) and 16 h pro-inflammatory cytokine-
14 stimulated conditions are shown with the grey, blue and red lines, respectively. Representative data
15 from HC1, HC3, MS1, and MS4 are shown from at least 2 independent differentiations. **(F)** The change in
16 geometric mean (Δ MFI = MFI staining – MFI isotype) of cell surface ICAM-1 as analyzed by flow
17 cytometry. **(C, D, F)** Bars show the mean of 6 clones from 3 HC or 7 clones from 4 MS patients. Each
18 symbol (HC: black, MS: red) represents the mean of at least two independent experiments using two
19 individual differentiations each performed in at least triplicates. Statistical analysis was performed as
20 outlined in Material and Methods. p-values are indicated in the respective figures.

21 **Figure 2. Impaired barrier characteristics in MS- versus HC-derived EECM-BMEC-like cells.**

22 **(A)** Immunofluorescence stainings of EECM-BMEC-like cells in co-culture with SMLC for 6 days are
23 shown. Junctions were stained for VE-cadherin, claudin-5, or occludin (red), and nuclei were stained
24 with DAPI (blue). Representative images of 3 HC and 4 MS from at least 3 independent experiments
25 using 3 individual differentiations performed on 3 distinct filters are shown. Yellow arrows indicate
26 visible disruptions of junctional stainings for claudin-5 and occludin. Scale bar = 50 μ m. **(B)** TEER of
27 EECM-BMEC-like cell monolayers derived from HC versus MS patients is shown. Black line represents
28 mean \pm SD of 6 clones from 3 HC and red line represents mean \pm SD of 7 clones from 4 MS-patients each
29 performed in triplicates and repeated at least twice using two individual differentiations for each donor.

1 **(C)** TEER at day 6 after seeding onto filters of EECM-BMEC-like cell monolayers derived from HC versus
 2 MS is shown. **(D, E)** Permeability of NaFl across EECM-BMEC-like cell monolayers: EECM-BMEC-like cells
 3 derived from HC (black) or MS patients (red) were cultured to confluency on 0.4 μm pore size Transwell
 4 filters in monoculture **(D)** or co-culture with SMLC from the same donor **(E)** for 6 days and permeability
 5 of NaFl was measured at day 6 after seeding onto the filter. **(C-E)** Bars show the mean of 6 clones from 3
 6 HC and 7 clones from 4 MS patients. Each symbol (HC: black, MS: red) shows the mean of at least two
 7 independent experiments using two individual differentiations each performed in at least triplicates.
 8 Statistical analysis was performed as outlined in Material and Methods. p-values are indicated in the
 9 respective figures.

10 **Figure 3. MS-derived EECM-BMEC-like cells show enhanced cell surface expression of ICAM-1 and**
 11 **VCAM-1**

12 **(A)** Immunofluorescence stainings of EECM-BMEC-like cell monolayers for ICAM-1, VCAM-1 (red) are
 13 shown. Nuclei were stained with DAPI (blue). Each staining is representative of at least 3 independent
 14 experiments using 3 individual differentiations performed on 3 distinct filters. NS and 1 ng/mL TNF- α +
 15 20 IU/mL IFN- γ stimulated conditions are shown. Scale bars = 50 μm . **(B)** Cell surface staining of EECM-
 16 BMEC-like cells for the adhesion molecules ICAM-1 and VCAM-1 was analyzed by flow cytometry.
 17 Isotype control, non-stimulated (NS), and 16 h pro-inflammatory cytokine-stimulated condition are
 18 shown in grey, blue, and red lines respectively. Representative data from HC1, HC2, MS1, and MS3 are
 19 shown. **(C)** The change in geometric mean ($\Delta\text{MFI} = \text{MFI staining} - \text{MFI isotype}$) of cell surface ICAM-1 and
 20 VCAM-1 of EECM-BMEC-like cells was analyzed by flow cytometry. Each symbol (HC: black, MS: red)
 21 represents the mean of at least two experiments using two independent differentiations. Bars show the
 22 mean of 6 clones from 3 HC and 7 clones from 4 MS. Statistical analysis was performed as outlined in
 23 Material and Methods. p-values are indicated in the respective figures.

24 **Figure 4. MS-derived EECM-BMEC-like cells support increased immune cells interaction**

25 **(A)** Schematic representation of the adhesion assay. **(B)** The number of allogeneic Th1* cells adherent to
 26 NS and pro-inflammatory cytokine-stimulated EECM-BMEC-like cell monolayers derived from HC versus
 27 MS patients was counted after 30 minutes under static conditions. In each assay, Th1* cell adhesion to
 28 EECM-BMEC-like cells from HC2 clone1 under NS conditions was included and the number of adherent
 29 Th1* cells/FOV was normalized to this condition (HC2 clone 1 NS condition = 1). **(C)** Schematic for *in*
 30 *vitro* live cell imaging of immune cell/BMEC interaction under physiological flow. **(D - G)** Analysis of the

1 arrest and post-arrest behavior of allogeneic Th1* cell or autologous PBMC interactions with pro-
2 inflammatory cytokine-stimulated EECM-BMEC-like cells in the field of view of the videos (example in
3 Supplementary video 1 and 2 for allogeneic Th1* and Supplementary video 3 and 4 for autologous
4 PBMCs) under physiological flow. **(D and F)** The number of allogeneic Th1* cells **(D)** or autologous
5 PBMCs **(F)** remaining arrested on the EECM-BMEC-like cell monolayer were quantified at the end of the
6 accumulation phase at 4 min 30 sec. The number of Th1* cells or PBMCs that had migrated across
7 EECM-BMEC-like cells were counted at 20 min. **(E and G)** Post-arrest allogeneic Th1* cell **(E)** or
8 autologous PBMCs **(G)** behavior on the EECM-BMEC-like cell monolayers under flow was analyzed. **(F**
9 **and G)** Autologous PBMCs from HC2 or MS3 were used in this assay. **(B, D-G)** Each symbol (HC: black,
10 MS: red) represents the mean of at least three experiments using two independent differentiations. Bars
11 show the mean of 6 clones from 3 HC and 7 clones from 4 MS. Statistical analysis was performed as
12 outlined in Material and Methods. p-values are indicated in the respective figures.

13 **Figure 5. Pre-activation of Wnt/ β -catenin signaling in MS-derived EECM-BMEC-like cells restores** 14 **barrier characteristics**

15 **(A)** Schematic representation of the Activation of the Wnt/ β -catenin signaling pathway in EPCs. **(B)**
16 Immunofluorescence staining for claudin-5 (red) and nuclei (DAPI, blue) of passage 3 EECM-BMEC-like
17 cells is shown. Representative images for clones derived from 4 MS patients of at least 3 independent
18 experiments using 3 individual differentiations performed on 3 distinct filters are shown. Yellow arrows
19 indicate disruptions in junctional claudin-5 staining. Scale bar = 50 μ m. **(C)** Permeability of NaFl across
20 passage 3 EECM-BMEC-like cell monolayers in the presence of absence of pre-treatment with 4 μ M
21 CHIR99021 are shown. **(D)** Cell surface staining of EECM-BMEC-like cells for the adhesion molecules
22 ICAM-1 and VCAM-1 in the presence of absence of pre-treatment with 4 μ M CHIR99021 under NS and
23 pro-inflammatory cytokines-stimulated condition was analyzed by flow cytometry. Isotype control,
24 DMSO control and CHIR99021 treatment condition are represented in grey, red, and green lines,
25 respectively. Representative data from MS1 – MS4 are shown. **(E)** The change in geometric mean (Δ MFI
26 = MFI staining – MFI isotype) of cell surface VCAM-1 of EECM-BMEC-like cells were analyzed by flow
27 cytometry. **(C, E)** Bars show the mean of 7 clones from 4 MS-patients. Each symbol represents the mean
28 of at least two independent experiments using two individual differentiations each performed in at least
29 triplicates. Statistical analysis was performed as outlined in Material and Methods. p-values are
30 indicated in the respective figures.

31

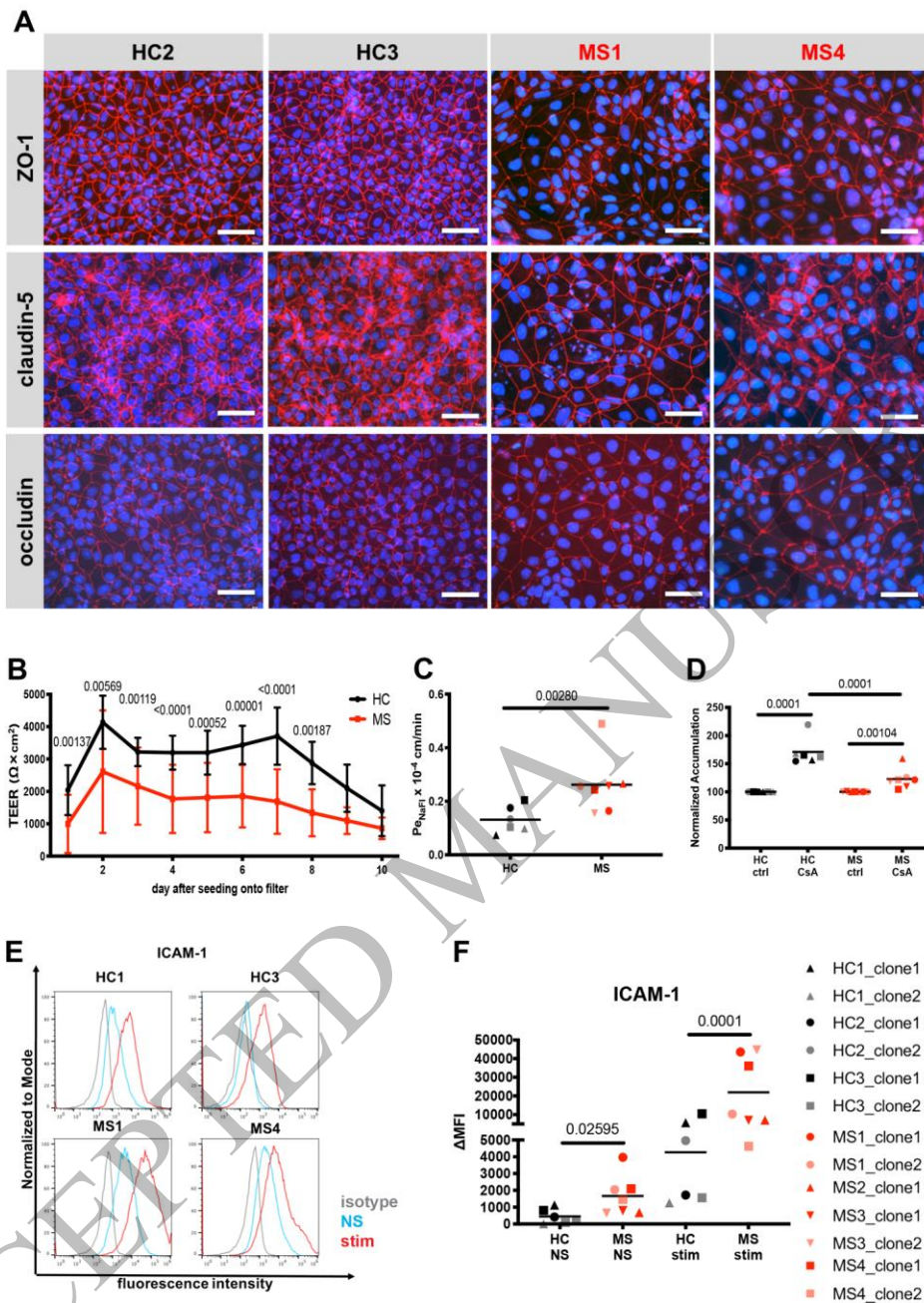


Figure 1
127x173 mm (6.5 x DPI)

1
2
3
4

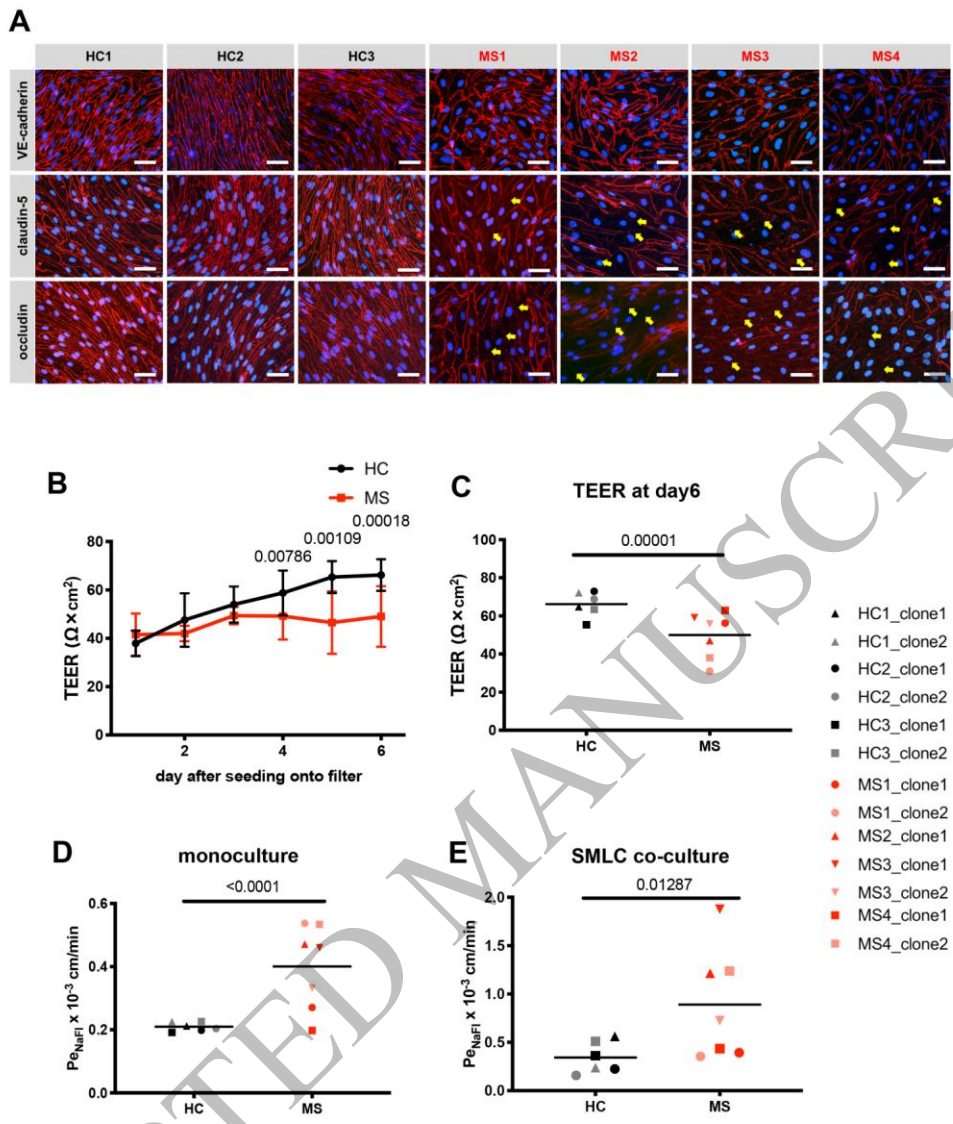


Figure 2
127x149 mm (6.5 x DPI)

1
2
3
4

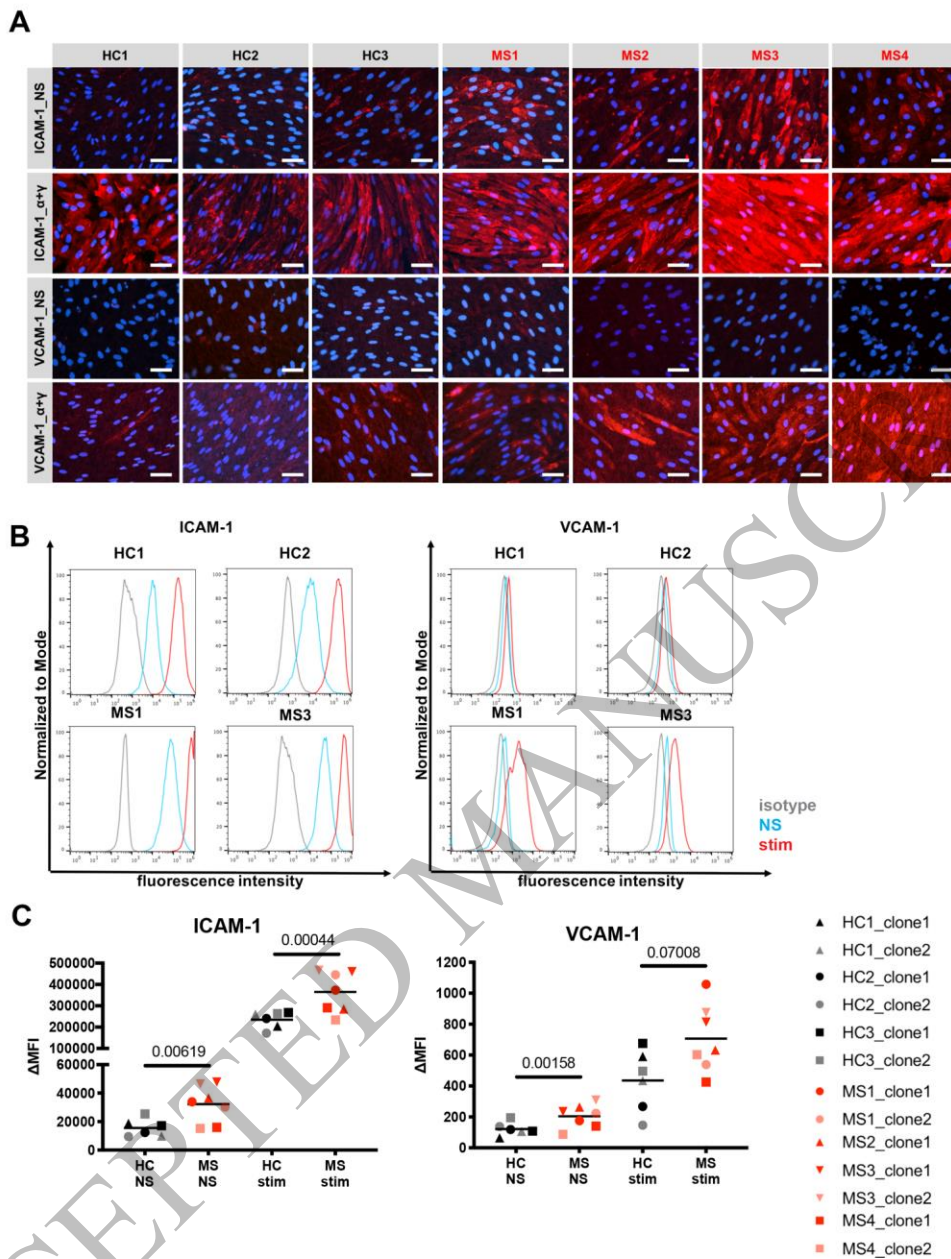


Figure 3
 127x167 mm (6.5 x DPI)

1
 2
 3
 4

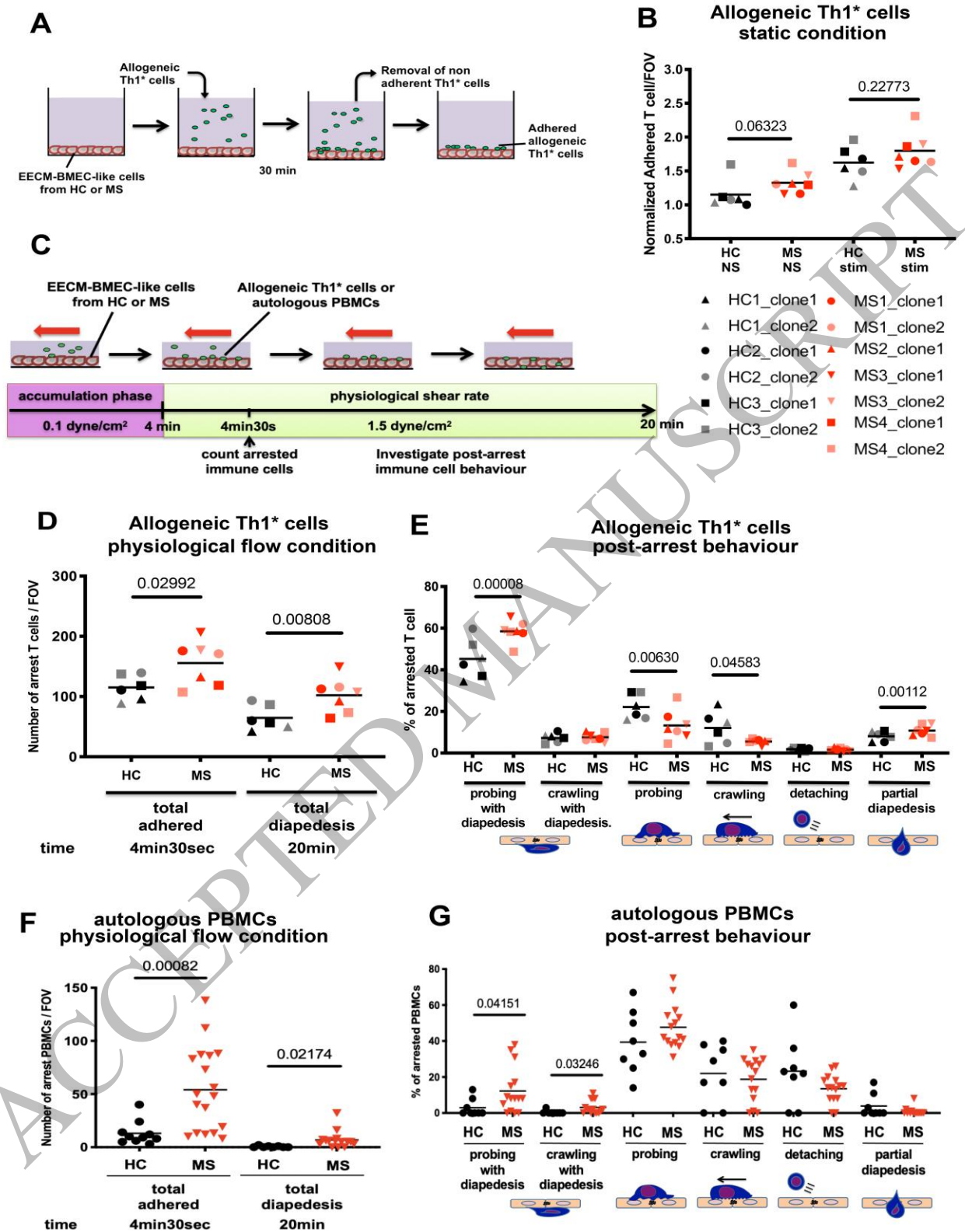


Figure 4
165x229 mm (6.5 x DPI)

1
2
3

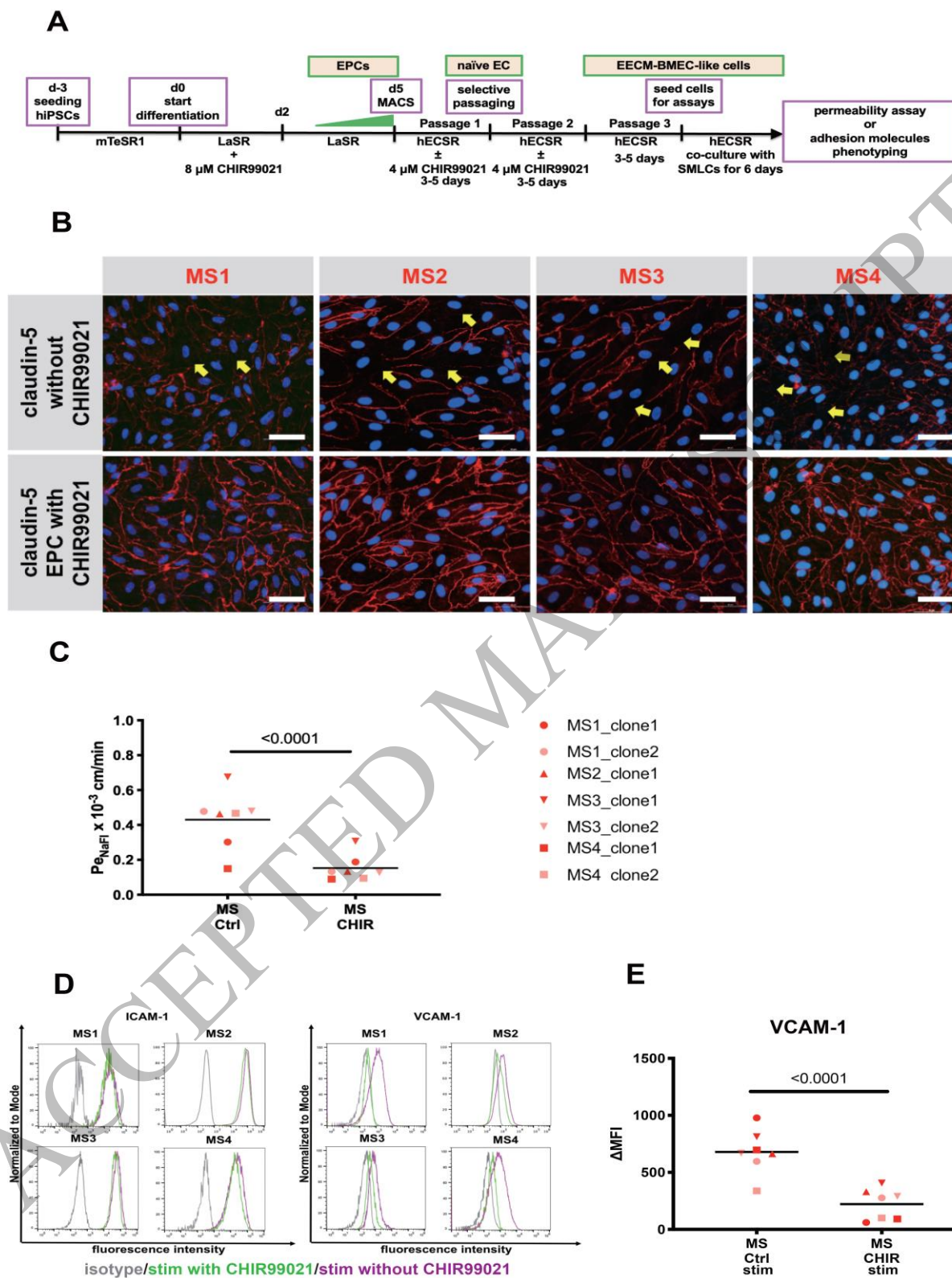


Figure 5
158x229 mm (6.5 x DPI)

1
2
3